

Natural Counterfactuals With Necessary Backtracking

Guang-Yuan Hao^{*1,2} Jiji Zhang^{*2} Biwei Huang³ Hao Wang⁴ Kun Zhang^{5,1}

Abstract

Counterfactual reasoning is pivotal in human cognition and especially important for providing explanations and making decisions. While Judea Pearl’s influential approach is theoretically elegant, its generation of a counterfactual scenario often requires interventions that are too detached from the real scenarios to be feasible. In response, we propose a framework of *natural counterfactuals* and a method for generating counterfactuals that are natural with respect to the actual world’s data distribution. Our methodology refines counterfactual reasoning, allowing changes in causally preceding variables to minimize deviations from realistic scenarios. To generate natural counterfactuals, we introduce an innovative optimization framework that permits but controls the extent of backtracking with a “naturalness” criterion. Empirical experiments indicate the effectiveness of our method.

1. Introduction

Counterfactual reasoning, which aims to answer what a feature of the world would have been if some other features had been different, is often used in human cognition, to perform self-reflection, provide explanations, and inform decisions. For AI systems to mirror such human-like decision-making processes, incorporating counterfactual reasoning is crucial. Judea Pearl’s structural approach to counterfactual modeling and reasoning stands as a cornerstone in machine learning (Pearl, 2009). Within this framework, counterfactuals are conceptualized as being generated by surgical interventions on the features to be changed that sever the original causal links responsible for those features, while

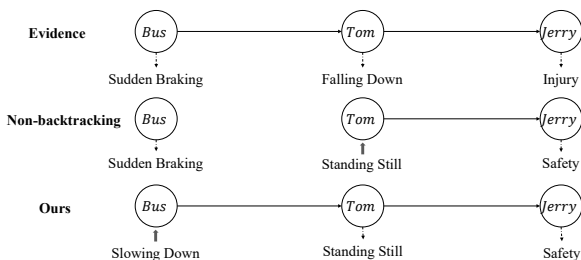


Figure 1. Motivational Example: Treating Bus, Tom, and Jerry as Variables. Downward arrows indicate their values, while upward arrows represent interventions.

leaving its causally upstream features untouched. Such non-backtracking counterfactual reasoning (i.e., reasoning about the consequences of an change without tracing back to changes in causally preceding variables) can yield valuable insights into the consequences of hypothetical actions. Consider a scenario: a sudden brake of a high-speed bus caused Tom to fall and injure Jerry, as illustrated in Fig. 1. Non-backtracking counterfactual reasoning would tell us that if Tom had stood still (despite the sudden braking), then Jerry would not have been injured. Pearl’s approach supplies a principled machinery to reason about conditionals of this sort, which are usually useful for explanation, planning, and responsibility allocation.

However, such surgical interventions may not be feasible in practice and may not provide significant assistance in self-reflection. In the previous example, preventing Tom’s fall in a sudden braking scenario requires defying mechanisms that are difficult or physically impossible to disrupt, such as the law of inertia. This supposed hard intervention may thus be too far-fetched to be relevant for practical purposes. For example, from a legal perspective, Tom’s fall causing Jerry’s injury could be given a “necessity defense,” acknowledging that the sudden braking left him with no alternatives (Conde, 1981). Hence, for the purpose of allocating responsibility, reasoning about the counterfactual situation of Tom standing still despite the sudden braking is arguably irrelevant or even misleading.

Our paper addresses counterfactual reasoning with a focus on outcomes that are constructive, which are intended to enhance practical situations and offer actionable insights. To achieve this, we ensure that every change in a system is natural. Thus, after these modifications, the new counterfactual

^{*}Equal contribution ¹Mohamed bin Zayed University of Artificial Intelligence ²The Chinese University of Hong Kong ³University of California San Diego ⁴Rutgers University ⁵Carnegie Mellon University. Correspondence to: Guang-Yuan Hao <guangyuanhao@outlook.com>, Jiji Zhang <jijizhang@cuhk.edu.hk>, Biwei Huang <bih007@ucsd.edu>, Hao Wang <hw488@cs.rutgers.edu>, Kun Zhang <kunz1@cmu.edu>.

data point will be natural with respect to data distribution in the actual world. Accordingly, we introduce the notion of “natural counterfactuals” to address the limitations of non-backtracking counterfactuals discussed above. For example, as depicted in Fig. 1, rather than the infeasible scenario where Tom does not fall at a sudden bus stop, a more realistic intervention would involve the bus slowing down earlier, achieved through backtracking (Lewis, 1979) that keeps the scenario within real-world bounds. Furthermore, one must ensure that the counterfactual data point remains as close as possible to the original data point; otherwise, unnecessary interventions may affect too many variables. To address this concern, we formulate a minimal change principle that guides us in performing only the necessary backtracking.

Moreover, from a machine learning perspective, when hard interventions lead to unrealistic scenarios relative to the training data, predicting counterfactual outcomes in such scenarios can be highly uncertain and inaccurate (Hassanpour & Greiner, 2019). This issue becomes particularly pronounced when non-parametric models are employed, as they often struggle to generalize to unseen, out-of-distribution data (Schölkopf et al., 2021). The risk of relying on such counterfactuals is thus substantial, especially in high-stake applications like healthcare and autonomous driving. To tackle this, we develop an approach that amounts to utilizing only feasible interventions that keep data within its original distribution, allowing backtracking when needed. This strategy effectively reduces the risk of inaccurate predictions and ensures more reliable results.

Consequently, our approach aims to achieve the goal of ensuring that counterfactual scenarios remain sufficiently realistic with respect to the actual world’s data distribution by permitting minimal yet necessary backtracking. It is designed on two major considerations: First, we need criteria to determine the feasibility of interventions, ensuring they are realistic with respect to actual-world data distribution. Second, we appeal to backtracking when and only when it is necessary to avoid infeasible interventions, and need to develop a feasible optimization framework to realize this strategy. The key contributions of this paper include:

- Developing a more flexible and realistic notion of natural counterfactuals, addressing the limitations of non-backtracking reasoning while keeping its merits as far as possible.
- Introducing an innovative and feasible optimization framework to generate natural counterfactuals.
- Detailing a machine learning approach to produce counterfactuals within this framework, with empirical results from simulated and real data showcasing the superiority of our method compared to non-backtracking counterfactuals.

2. Related Work

Non-backtracking Counterfactual Generation. As will become clear, our theory is presented in the form of counterfactual sampling or generation. (Ribeiro et al., 2023; Kocaoglu et al.; Dash et al., 2022; Sanchez & Tsafaris) use the deep generative models to learn an SCM from data given a causal graph; these works strictly follow Pearl’s theory of non-backtracking counterfactuals. Our case studies will examine some of these models and demonstrate their difficulties in dealing with interventions that are unrealistic relative to training data.

Backtracking Counterfactuals. Backtracking in counterfactual reasoning has drawn plenty of attention in philosophy (Hiddleston, 2005), psychology (Dehghani et al., 2012), and cognitive science (Gerstenberg et al., 2013). Hiddleston (2005) proposes a theory that is in spirit similar to ours, in which backtracking is allowed but limited by some requirement of matching as much causal upstream as possible. Gerstenberg et al. (2013) shows that people use both backtracking and non-backtracking counterfactuals in practice and tend to use backtracking counterfactuals when explicitly required to explain causes for the supposed change in a counterfactual. von Kügelgen et al. (2022) is a most recent paper explicitly on backtracking counterfactuals. The main differences between that work and ours are that von Kügelgen et al. (2022) requires backtracking all the way back to exogenous noises and measures closeness on noise terms, which are less desirable than limiting backtracking to what we call “necessary backtracking” and measuring closeness directly on endogenous, observable variables, because changes to the unobserved or noise terms are by definition outside of our control and not actionable. Moreover, their backtracking counterfactuals sometimes allow gratuitous changes, as we explain in Sec. G of the Appendix.

Counterfactual Explanations. A prominent approach in explainable AI is counterfactual explanation (Wachter et al., 2018; Dhurandhar et al., 2018; Mothilal et al., 2020; Barocas et al., 2020; Verma et al., 2020; Schut et al., 2021), on which our work is likely to have interesting bearings. Most works on this topic define some sense of minimal changes of an input sample with a predicted class c such that adding the minimal changes into the input would make it be classified into another (more desirable) class. Although this paper does not discuss counterfactual explanations, our framework may well be used to define a novel notion of counterfactual explanation by requiring the counterfactual instances to be “natural” in our sense.

3. Notations and Background

In this section, we begin by outlining various basic concepts in causal inference, followed by an introduction to non-backtracking counterfactuals.

Structural Causal Models. We use a structural causal model (SCM) to represent the data generating process of a causal system. A SCM is a mathematical structure consisting of a triplet $\mathcal{M} := \langle \mathbf{U}, \mathbf{V}, \mathbf{F} \rangle$, with an exogenous (noise) variable set $\mathbf{U} = \{\mathbf{U}_1, \dots, \mathbf{U}_N\}$, an endogenous (observed) variable $\mathbf{V} = \{\mathbf{V}_1, \dots, \mathbf{V}_N\}$, and a function set $\mathbf{f} = \{f_1, \dots, f_N\}$ (Pearl, 2009). Each function, $f_i \in \mathbf{f}$, specifies how an endogenous variable \mathbf{V}_i is determined by its parents $\mathbf{PA}_i \subseteq \mathbf{V}$:

$$\mathbf{V}_i := f_i(\mathbf{PA}_i, \mathbf{U}_i), \quad i = 1, \dots, N \quad (1)$$

Local Mechanisms. A local mechanism is the conditional distribution of an endogenous variable based on its parent variables, represented as $p(\mathbf{V}_i | \mathbf{PA}_i)$ for $i = 1, \dots, N$. This definition inherently captures the properties of noise variables; given a fixed value for \mathbf{PA}_i , noise \mathbf{U}_i entirely dictates the probability of \mathbf{V}_i (Pearl, 2009). Hence, throughout this paper, the term “local mechanisms” will encompass both the conditional distribution of an endogenous variable given its parents $p(\mathbf{V}_i | \mathbf{PA}_i)$ and the distribution of the noise variable $p(\mathbf{U}_i)$.

Intervention. Given an SCM, an intervention on an endogenous variable \mathbf{A} is represented by replacing its function with a constant function $\mathbf{A} = \mathbf{a}^*$, where \mathbf{a}^* is the target value of \mathbf{A} , and leaving functions and local mechanisms for other variables intact (Pearl, 2009).

Non-Backtracking Counterfactuals. A counterfactual ponders what would happen in a scenario that differs from the actual one in a certain way. Following a standard notation, terms with a $*$ superscript refer to a counterfactual world. For example, \mathbf{u}_i^* denotes \mathbf{U}_i ’s value in a counterfactual world. Let \mathbf{A} , \mathbf{B} , and \mathbf{E} be endogenous variables. Here is a general counterfactual question: given evidence $\mathbf{E} = \mathbf{e}$, what would the value of \mathbf{B} have been if \mathbf{A} had been \mathbf{a}^* ? The Pearlian, non-backtracking reading of this question takes the counterfactual supposition of $\mathbf{A} = \mathbf{a}^*$ to be realized by an intervention on \mathbf{A} (Pearl, 2009). Given this understanding, counterfactual inference includes three steps. (1) Abduction: The noise distribution is updated based on the evidence $\mathbf{E} = \mathbf{e}$. (2) Action: The causal model is modified, in which \mathbf{A} is fixed to \mathbf{a}^* while keeping other components the same as before. (3) Prediction: The counterfactual outcome of \mathbf{B} is inferred using the updated noise distribution and the modified model.

4. A Framework for Natural Counterfactuals

Do(\cdot) and Change(\cdot) Operators. In considering a counterfactual scenario in which \mathbf{A} ’s value is \mathbf{a}^* instead of \mathbf{a} , the non-backtracking mode always appeals to a direct intervention on \mathbf{A} , i.e., $do(\mathbf{A} = \mathbf{a}^*)$ in Pearl’s influential notation. However, in our framework, the counterfactual supposition is not necessarily realized by a direct intervention on \mathbf{A} , and may be realized by interventions on some

causally preceding variables, depending on the “naturalness” of interventions. To differentiate from the intervention $do(\mathbf{A} = \mathbf{a}^*)$ in non-backtracking counterfactuals, we introduce a specific operator $change(\cdot)$ and $change(\mathbf{A} = \mathbf{a}^*)$ signifies a desired modification in \mathbf{A} , which may result from an intervention on \mathbf{A} or an intervention on some causal ancestors of \mathbf{A} .

We introduce two new concepts to determine where to carry out feasible interventions on \mathbf{C} (either \mathbf{A} itself or the causal earlier variables of \mathbf{A}) to realize $change(\mathbf{A} = \mathbf{a}^*)$ in natural counterfactuals: a naturalness constraint and a necessary backtracking principle.¹ First, we propose using a naturalness criterion to assess the feasibility of an intervention. We assume that actual-world data contain all relevant causal mechanisms for a given causal graph; thus, out-of-distribution data are physically infeasible. This means we limit changed values resulting from interventions to stay within the observed data distribution, ensuring the feasibility of interventions on \mathbf{C} and the naturalness of resulting counterfactuals.

Furthermore, we consider the proximity between the actual value and its counterfactual value, leading to a principle known as “necessary backtracking.” This principle aims to minimize changes in the counterfactual world and backtrack as little as possible, keeping \mathbf{C} as closely aligned with \mathbf{A} as feasible. In summary, the naturalness constraint and necessary backtracking both contribute to determining a feasible intervention.

4.1. Feasible Intervention Optimization

To address the challenge of determining a feasible intervention, we propose treating it as an optimization problem. This entails optimizing a defined distance metric between the counterfactual outcome produced by the intervention and the corresponding real-world data point, following the principle of necessary backtracking. This optimization procedure also enforces a naturalness constraint on counterfactuals. We define this optimization framework as Feasible Intervention Optimization (FIO) as follows:

$$\begin{aligned} & \underset{an(\mathbf{A})^*}{\text{minimize}} && D(an(\mathbf{A}), an(\mathbf{A})^*) \\ & \text{s.t.} && \mathbf{A} = \mathbf{a}^*, \\ & && g_n(an(\mathbf{A})^*) > \epsilon. \end{aligned} \quad (2)$$

where $an(\mathbf{A})$ and $an(\mathbf{A})^*$ represent the actual value and counterfactual value of \mathbf{A} ’s ancestors $\mathbf{AN}(\mathbf{A})$ respectively, where $\mathbf{A} \in \mathbf{AN}(\mathbf{A})$. $D(\cdot)$ is a specific distance metric to

¹Given a feasible intervention, our natural counterfactual inference also follows three steps: abduction, action, and prediction, aligned with the procedure of non-backtracking counterfactuals as mentioned in Sec. 3. More details for the procedure of natural counterfactuals are in Sec. E.

assess the distance between actual world and counterfactual world. $g_n(\cdot)$ measures the naturalness of counterfactual value of \mathbf{A} 's ancestors and ϵ is a small constant. We will discuss $D(\cdot)$ and $g_n(\cdot)$ later.

Optimization Scope. All possible backtracking variables are contained within \mathbf{A} 's ancestor set $\mathbf{AN}(\mathbf{A})$. Consequently, our optimization focus remains confined to these nodes. Through FIO, we obtain the optimal value $an(\mathbf{A})^*$. This identifies the changed variables, \mathbf{C} , which we target for intervention, enabling the definition of the feasible intervention $do(\mathbf{C} = \mathbf{c}^*)$, with \mathbf{c}^* as the post-optimization counterfactual values of \mathbf{C} .

Naturalness Constraint. In addition to ensuring the change $\mathbf{A} = \mathbf{a}^*$, the counterfactual value $an(\mathbf{A})^*$ must satisfy a naturalness criterion to ensure the feasibility of interventions. Specifically, its naturalness should exceed the threshold ϵ to remain within the data distribution. A detailed discussion of potential naturalness constraints is presented in Sec. 4.2.

Distance Measure $D(\cdot)$. $D(\cdot)$ considers the concept of necessary backtracking and serves as a metric for quantifying the distance between the counterfactual and actual worlds. For a detailed exploration, please refer to Sec. 4.3.

4.2. Naturalness Constraints

To ensure an intervention's feasibility, we stipulate that the resulting counterfactual value $an(\mathbf{A})^*$ should fall within the data distribution, thus being natural relative to this distribution. We introduce a naturalness criterion, which confines the feasible support for $an(\mathbf{A})^*$ in Eqn. 2 of the FIO framework.

Intuitively, the more frequently a value occurs, the more "natural" it is considered. Therefore, we assess this naturalness by examining the distribution characteristics, such as density, of each variable's value $\mathbf{V}_j = \mathbf{v}_j^*$ within $\mathbf{AN}(\mathbf{A})$. This assessment is relative to the variable's local mechanism $p(\mathbf{V}_j | pa_j^*)$, where $\mathbf{V}_j \in \mathbf{AN}(\mathbf{A})$ and pa_j^* denotes the parent value of \mathbf{V}_j . Specifically, our approach determines whether the density of \mathbf{v}_j^* surpasses a pre-established threshold ϵ , utilized as a standard for appraising naturalness.²

4.2.1. LOCAL NATURALNESS CRITERIA

Indeed, it might be difficult to find a universal definition for naturalness criteria, and thus, various criteria for naturalness can be explored. This allows for a more tailored approach to assessing naturalness in different contexts or applications. We start by assessing the naturalness of one variable's value,

²The concept of "naturalness" can have various interpretations. In our context, it is defined by the data distribution in Structural Causal Models (SCMs). We do not claim that this is the only or uniquely best interpretation, but that it is a useful one to study and deploy.

\mathbf{v}_j^* , within the counterfactual data point $an(\mathbf{A})^*$ in this section, followed by an examination of the overall naturalness of $an(\mathbf{A})^*$ in the next section.

We introduce "local ϵ -natural generation," where a value satisfies this criterion if it is a natural outcome of its local mechanism. We focus on a specific value $\mathbf{V}_j = \mathbf{v}_j^*$, alongside its parent value $\mathbf{PA}_j = pa_j^*$, noise value $\mathbf{U}_j = \mathbf{u}_j^*$, and the corresponding local mechanism, expressed by $p(\mathbf{V}_j | \mathbf{PA}_j = pa_j^*)$ or $p(\mathbf{U}_j)$. The cumulative distribution function (CDF) for noise variable \mathbf{U}_j at $\mathbf{U}_j = \mathbf{u}_j^*$ is $F(\mathbf{u}_j^*) = \int_{-\infty}^{\mathbf{u}_j^*} p(\mathbf{U}_j) d\mathbf{U}_j$, and for the conditional distribution $p(\mathbf{V}_j | \mathbf{PA}_j = pa_j^*)$ at $\mathbf{V}_j = \mathbf{v}_j^*$ is $F(\mathbf{V}_j | pa_j^*) = \int_{-\infty}^{\mathbf{v}_j^*} p(\mathbf{V}_j = \mathbf{v}_j^* | pa_j^*) d\mathbf{V}_j$.

We propose the following potential criteria based on entropy-normalized density, CDF of exogenous variables, and CDF of conditional distributions. The entropy-normalized naturalness measure evaluates the naturalness of \mathbf{v}_j^* in relation to its local mechanism $p(\mathbf{V}_j | \mathbf{PA}_j = pa_j^*)$. The CDF-based measures, namely the latter two criteria, consider data points in the tails to be less natural. Each of these criteria has its own intuitive appeal, and their relative merits will be discussed subsequently. We formally establish the three criteria as follows:

- (1) Entropy-Normalized Measure: $p(\mathbf{v}_j^* | pa_j^*) e^{H(\mathbf{V}_j | pa_j^*)} > \epsilon$, where $H(\mathbf{V}_j | pa_j^*) = \mathbb{E}[-\log p(\mathbf{V}_j | pa_j^*)]$;
- (2) Exogenous CDF Measure: $\min(F(\mathbf{u}_j^*), 1 - F(\mathbf{u}_j^*)) > \epsilon$, i.e., $\epsilon < F(\mathbf{u}_j^*) < 1 - \epsilon$;
- (3) Conditional CDF Measure: $\min(F(\mathbf{v}_j^* | pa_j^*), 1 - F(\mathbf{v}_j^* | pa_j^*)) > \epsilon$, i.e., $\epsilon < F(\mathbf{v}_j^* | pa_j^*) < 1 - \epsilon$.

where the function $\min(\cdot)$ returns the minimum value between two given values.

Choice (1): Entropy-Normalized Measure. Specifically, Choice (1), $p(\mathbf{v}_j^* | pa_j^*) e^{H(\mathbf{V}_j | pa_j^*)}$, can be rewritten as $e^{\log(p(\mathbf{v}_j^* | pa_j^*)) + \mathbb{E}[-\log p(\mathbf{V}_j | pa_j^*)]}$, where $-\log(p(\mathbf{v}_j^* | pa_j^*))$ can be seen as the measure of surprise of \mathbf{v}_j^* given pa_j^* and $\mathbb{E}[-\log p(\mathbf{V}_j | pa_j^*)]$ can be considered as the expectation of surprise of the local mechanism $p(\mathbf{V}_j | pa_j^*)$ (Ash, 2012). Hence, the measure is the relative naturalness (i.e., negative surprise) of \mathbf{V}_j . Implementing this measure may be straightforward when employing a parametric SCM where the conditional distribution can be explicitly represented.

Choice (2): Exogenous CDF Measure. If using a parametric SCM, we might directly measure differences on exogenous variables. However, in a non-parametric SCM, exogenous variables are not identifiable, and different noise variables may have different distributions. Hence, we choose to use the CDF of exogenous variables to align the naturalness

of different distributions, based on a common assumption to achieve non-parametric SCMs in the machine learning system. Under the assumption, the support of the local mechanism $p(\mathbf{V}_j | \mathbf{PA}_j = pa_j^*)$ does not contain disjoint sets, and a nonlinear, non-parametric model $\mathbf{V}_j = f_j(pa_j^*, \mathbf{U}_j)$ is implemented, where f is monotonically increasing with respect to \mathbf{U}_j . Noise \mathbf{U}_j usually assumed to be a standard Gaussian (Lu et al., 2020). In this way, counterfactuals are identifiable, discussed in Sec. 4.4. Data points from the tails of a standard Gaussian can be thought of as less improbable events. Hence, $\mathbf{V}_j = \mathbf{v}_j^*$ satisfies local ϵ -natural generation when its exogenous CDF $F(\mathbf{u}_j^*)$ falls within the range $(\epsilon, 1 - \epsilon)$. In practice, for a single variable, \mathbf{U}_j is a one-dimensional variable, and it is easier to enforce the measure than Choice (1), which involves conditional distributions.

Choice (3): Conditional CDF Measure. The measure treats a particular value in the tails of local mechanism $p(\mathbf{V}_j | pa_j^*)$ as unnatural. Hence, $\mathbf{V}_j = \mathbf{v}_j^*$ meets local ϵ -natural generation when $F(\mathbf{V}_j = \mathbf{v}_j^* | pa_j^*)$ falls within the range $(\epsilon, 1 - \epsilon)$ instead of tails. This measure can be used in parametric models where the conditional distribution can be explicitly represented. Notice, it can be easily used in non-parametric models when those models satisfy the assumption mentioned in Choice (2), and the measure is equivalent to Choice (2), since the CDF $F(X | pa_j^*)$ has a one-to-one mapping with the CDF $F(\mathbf{U}_j)$, i.e., $F(\mathbf{v}_j^* | pa_j^*) = F(\mathbf{u}_j^*)$, when $\mathbf{v}_j^* = f(pa_j^*, \mathbf{u}_j^*)$.

4.2.2. ϵ -NATURAL GENERATION

Based on the definition of local ϵ -natural generation, we can define ϵ -natural generation to judge whether the counterfactual value $an(\mathbf{A})^*$ is natural.

Definition 1 (ϵ -Natural Generation). *Given a SCM containing a set \mathbf{A} . A set $\mathbf{AN}(\mathbf{A})$ contains all ancestors of \mathbf{A} and \mathbf{A} itself. Data point $\mathbf{AN}(\mathbf{A}) = an(\mathbf{A})^*$ satisfies ϵ -natural generation, if and only if, for any variable $\mathbf{V}_j \in \mathbf{AN}(\mathbf{A})$, $\mathbf{V}_j = \mathbf{v}_j^*$ satisfies local ϵ -natural generation, where \mathbf{v}_j^* is the value of \mathbf{V}_j and ϵ is a small constant.*

where the definition of local ϵ -natural generation could be one of the optional definitions in 4.2.1 and a larger value of ϵ implies a higher standard for the naturalness of the generated data point $an(\mathbf{A})^*$. To make intervention feasible, we require $an(\mathbf{A})^*$ to meet ϵ -natural generation.

4.3. Distance Measure for Necessary Backtracking

The naturalness constraints outlined in Eqn. 2 were comprehensively addressed previously. We now focus on defining the necessary backtracking distance in Eqn. 2 of the FIO framework to minimize the change in the counterfactual data point. Our analysis introduces two distinct definitions of distance in the counterfactual context. The first prioritizes

minimizing changes in observable variables to minimize perceptible differences post-intervention. The second focuses on reducing alterations in local mechanisms, recognizing them as the inherent cost of intervention. Due to space limitations, we will primarily elaborate on minimal changes in observable variables. A more thorough investigation of changes in local mechanisms can be found in Sec. H.

Minimal Change in Observable Variables. The differences in perception are closely tied to the alterations in the values of observable (endogenous) variables resulting from the intervention. Intuitively, the total distance is the aggregate of distances across various variables in the ancestor set $\mathbf{AN}(\mathbf{A})$. Therefore, we utilize the L^1 norm to measure this distance, as the L^1 norm offers the advantage of additive distances across variables. We define this distance as the **perception distance**:

$$D(an(\mathbf{A}), an(\mathbf{A})^*) = \|an(\mathbf{A}) - an(\mathbf{A})^*\|_1 \quad (3)$$

where $an(\mathbf{A})$ and $an(\mathbf{A})^*$ represent the actual value and counterfactual value of \mathbf{A} 's ancestors $\mathbf{AN}(\mathbf{A})$ respectively, where $\mathbf{A} \in \mathbf{AN}(\mathbf{A})$. Because endogenous variables may vary in scale, we utilize the standard deviation of variables to normalize each endogenous variable before computing the distance. This normalization ensures a consistent and fair evaluation of changes across all variables, irrespective of their individual scales.

Implicitly, our distance metric favors changes in variables that are as proximal as possible to the target variable \mathbf{A} , since altering a more preceding variable typically results in changes to more downstream variables. When the value $an(\mathbf{A})^*$, resulting from a hard intervention on \mathbf{A} , meets the ϵ -natural generation criterion, it suggests that our distance metric $D(an(\mathbf{A}), an(\mathbf{A})^*)$ becomes minimal, i.e., $|\mathbf{a} - \mathbf{a}^*|$. This effectively eliminates the need for backtracking in such cases. However, If a hard intervention does not meet the ϵ -natural generation criterion, it becomes necessary to backtrack.

4.4. Identifiability of Natural Counterfactuals

In practice, we often do not know the form of structural equation models and noise variables are not identifiable from the observed variables. Hence, we assume causal structural models satisfy the conditions of the following theorem derived from Theorem 1 of Lu et al. (2020) with proof in Sec. B, under which natural counterfactuals are identifiable with unknown structural equation models.

Theorem 4.1 (Identifiable Counterfactuals). *Suppose \mathbf{V}_i satisfies the following structural causal model: $\mathbf{V}_i := f_i(\mathbf{PA}_i, \mathbf{U}_i)$ for any $\mathbf{V}_i \in \mathbf{V}$, where $\mathbf{U}_i \perp \mathbf{PA}_i$ and assume unknown f_i is smooth and strictly monotonic w.r.t. \mathbf{U}_i for fixed values of \mathbf{PA}_i . If we have evidence $\mathbf{E} = \mathbf{e}$, with an intervention $do(\mathbf{C} = \mathbf{c}^*)$, the counterfactual distribution*

of \mathbf{B} is identifiable; that is, $p(\mathbf{B} \mid do(\mathbf{C} = \mathbf{c}^*), \mathbf{E} = \mathbf{e})$ is identifiable.³

Following Feasible Intervention Optimization, we obtain the feasible intervention $do(\mathbf{C} = \mathbf{c}^*)$. This theorem ensures the identifiability of our natural counterfactuals given $do(\mathbf{C} = \mathbf{c}^*)$, under the stated assumptions. Note that the assumptions do not require more information on the structural functions or on the noise distributions. Hence, even without full information about the SCM, we can still use conditional distributions to infer natural counterfactuals, as well as non-backtracking counterfactuals, if the assumptions of the above theorem hold.

5. A Method for Generating Natural Counterfactuals

In this section, we provide a practical method for integrating natural counterfactuals into a machine learning system. In our scenario, we start with real-world data and a causal graph, lacking the SCM. We employ a non-parametric model to model the conditional distributions of endogenous variables and consider the model as a non-parametric SCM, making the assumption that each noise variable adheres to a standard Gaussian distribution. This learned SCM serves as the basis for generating natural counterfactuals.

To implement a particular method, we plug perception distance (Eqn. 3) and naturalness constraint (Choice (3) in Sec. 4.2.1) into Eqn. 2 of the FIO framework. Below is the equation of optimization:

$$\begin{aligned} & \underset{an(\mathbf{A})^*}{\text{minimize}} \|an(\mathbf{A}) - an(\mathbf{A})^*\|_1 \\ & \text{s.t. } \mathbf{A} = \mathbf{a}^*, \\ & \quad \epsilon < F(\mathbf{V}_j = \mathbf{v}_j^* | pa_j^*) < 1 - \epsilon, \forall \mathbf{V}_j \in \mathbf{AN}(\mathbf{A}). \end{aligned} \quad (4)$$

Notice that the equation could have no solutions, i.e., there is no feasible intervention, when the two constraints impossibly hold at the same time. In practice, the Lagrangian method (Boyd & Vandenberghe, 2004) is used to optimize our objective loss as below:

$$\begin{aligned} \mathcal{L} &= \|an(\mathbf{A}) - an(\mathbf{A})^*\|_1 + \\ & w_\epsilon \sum_j [\max(\epsilon - F(\mathbf{V}_j = \mathbf{v}_j^* | pa_j^*), 0) + \max(\epsilon + F(\mathbf{V}_j = \mathbf{v}_j^* | pa_j^*) - 1, 0)] \\ & \text{s.t. } \mathbf{A} = \mathbf{a}^* \end{aligned} \quad (5)$$

where the function $\max(\cdot)$ returns the maximum value between two given values. The first term represents the mea-

³If the assumption does not hold, identifiability may fail. For example, for $Y = XU_1 + U_2$ where Y and X are endogenous variables and U_1 and U_2 are noise, the counterfactual outcome is not identifiable. Similarly, our approach can be applied to discrete variables satisfying the assumption of counterfactual stability developed by (Oberst & Sontag, 2019) in theory.

sure of distance between two distinct worlds, while the second term enforces the constraint of ϵ -natural generation. Here, the constant hyperparameter w_ϵ serves to penalize noise values situated in the tails of noise distributions.

6. Case Studies

In this section, we apply our method and evaluate its effectiveness through empirical experiments on four synthetic datasets and two real-world datasets: MorphoMNIST and 3DIdentBOX.

We propose using the difference between generated and actual outcomes as a measure of performance. We expect our natural counterfactuals to significantly reduce error compared to non-backtracking counterfactuals. This advantage can be attributed to the effectiveness of our method in performing necessary backtracking that identifies feasible interventions, keeping counterfactual values within the data distribution, particularly when direct interventions are not feasible. On the other hand, non-backtracking counterfactuals, relying solely on direct interventions, often produce out-of-distribution values, posing challenges for machine learning model generalization.

6.1. Simulation Experiments

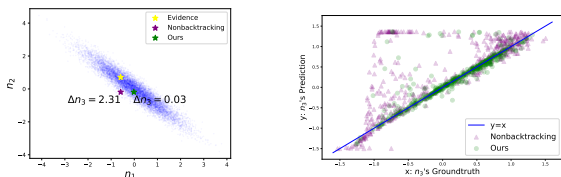
We start with four simulation datasets, which we use designed SCMs to generate. Please refer to the Appendix for more details about these datasets. Let first devolve into *Toy I*, which contains three variables (n_1, n_2, n_3) . n_1 is the confounder of n_2 and n_3 , and n_1 and n_2 causes n_3 .

Experimental Settings. Assume data and a causal graph are known, but not the ground-truth SCMs. We employ normalizing flows to capture the causal mechanisms of variables (n_1, n_2, n_3) . Given the learned SCMs and a data point from the test set as evidence, we set n_1 or n_2 as target variable \mathbf{A} and randomly sample values from test dataset as counterfactual values of the target variable n_1 or n_2 . For our natural counterfactuals, we use Eqn. 5 to determine feasible interventions, with $\epsilon = 10^{-4}$ and $w_\epsilon = 10^4$. In non-backtracking counterfactuals, n_1 or n_2 is directly intervened on. We report the Mean Absolute Error (MAE) between our learned counterfactual outcomes and ground-truth outcomes on n_2 or/and n_3 with multiple random seeds. Notice there may be no feasible interventions for some changes, as we have claimed in Sec. 5, and thus we only report outcomes with feasible interventions, which is within the scope of our natural counterfactuals.

Visualization of Counterfactuals on a Single Sample. We assess the counterfactual outcomes for a sample $(n_1, n_2, n_3) = (-0.59, 0.71, -0.37)$, aiming for $change(n_2 = 0.19)$. In Fig. 2 (a), we depict the original data point (yellow), the non-backtracking counterfactual (purple), and the natural counterfactual (green) for (n_1, n_2) .

Table 1. MAE Results on Toy 1 – 4. For simplicity, we use *do* operator in the table to save room, and when natural counterfactuals are referred to, *do* means *change*. Our approach exhibits an obvious MAE reduction when applied to n_2 as expected.

Dataset	Toy 1		Toy 2		Toy 3				Toy 4				
<i>do</i> or <i>change</i>	do(n_1)	do(n_2)	do(n_1)	do(n_2)	do(n_1)	do(n_2)	do(n_3)	do(n_1)	do(n_2)	do(n_3)			
Outcome	n_2	n_3	n_3	n_2	n_2	n_3	n_4	n_3	n_4	n_4	n_2	n_3	n_3
Nonbacktracking	0.477	0.382	0.297	0.315	0.488	0.472	0.436	0.488	0.230	0.179	0.166	0.446	0.429
Ours	0.434	0.354	0.114	0.303	0.443	0.451	0.423	0.127	0.136	0.137	0.158	0.443	0.327



(a) Outcome error on a single sample (b) Groundtruth-Prediction Scatter Plot

Figure 2. The Visualization Results on Toy 1 (View the enlarged figure in Fig. 7 in the Appendix).

The ground-truth support for these variables is shown as a blue scatter plot.

(1) *Feasible Intervention VS Hard Intervention.* Non-backtracking counterfactuals apply a hard intervention on n_2 ($do(n_2 = 0.19)$), shifting the evidence (yellow) to the post-intervention point (purple), which lies outside the support of (n_1, n_2) . This implies that direct interventions can result in unnatural values. Conversely, our natural counterfactual (green) remains within the support of (n_1, n_2) due to necessary backtracking and feasible intervention on n_2 .

(2) *Outcome Error.* We calculate the absolute error between n_3 's model prediction and ground-truth value using either the green or purple point as input for the model $p(n_3 | n_1, n_2)$. The error for the green point is significantly lower at 0.03, compared to 2.31 for the purple point. This lower error with the green point is because it stays within the data distribution after a feasible intervention, allowing for better model generalization than the out-of-distribution purple point.

Counterfactuals on Whole Test Set. In Fig. 2 (b), we illustrate the superior performance of our counterfactual method on the test set, notably outperforming non-backtracking counterfactuals. This is evident as many outcomes from non-backtracking counterfactuals for n_3 significantly diverge from the $y = x$ line, showing a mismatch between predicted and ground-truth values. In contrast, our method's outcomes largely align with this line, barring few exceptions possibly due to learned model's imperfections. This alignment is attributed to our method's consistent and feasible interventions, enhancing prediction accuracy, while non-backtracking counterfactuals often lead to infeasible results. Table 1 supports these findings, demonstrating that our approach exhibits a MAE reduction of 61.6% when applied to n_2 , compared with the non-backtracking method.

Table 2. Ablation Study on ϵ

Model	ϵ	CFs	do(t)		do(i)	
			t	i	t	i
V-SCM	-	NB	0.336	4.532	0.283	6.556
	10^{-4}	Ours	0.314	4.506	0.171	4.424
	10^{-3}		0.298	4.486	0.161	4.121
	10^{-2}		0.139	4.367	0.145	3.959
H-SCM	-	NB	0.280	2.562	0.202	3.345
	10^{-4}	Ours	0.260	2.495	0.105	2.211
	10^{-3}		0.245	2.442	0.096	2.091
	10^{-2}		0.093	2.338	0.083	2.063

Furthermore, our method excels even when intervening in the case of n_1 , a root cause, by excluding points that do not meet the ϵ -natural generation criteria, further demonstrating its effectiveness.

Additional Causal Graph Structures. Our method also shows superior performance on three other simulated datasets with varied causal graph structures (Toy 2 to Toy 4), as demonstrated in Table 1.

6.2. MorphoMNIST

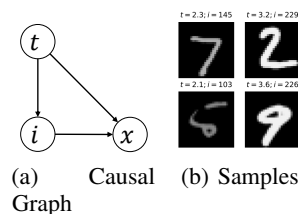


Figure 3. Causal Graph and samples of Morpho-MNIST.

MorphoMNIST (Castro et al., 2019) involves three variables (t, i, x) . As depicted in Fig. 3 (a), t (digit stroke thickness) causes both i (stroke intensity) and x (images), with i being the direct cause of x .

In our experiments, mirroring those in Section 6.1, we incorporate two key changes. First, we utilize two advanced deep learning models, V-SCM (Pawlowski et al., 2020) and H-SCM (Ribeiro et al., 2023), for doing counterfactuals. Second, due to the absence of ground-truth SCM for assessing outcome error, we adopt the **counterfactual effectiveness** metric from (Ribeiro et al., 2023), as developed in (Monteiro et al., 2023). This involves training a predictor on the dataset to estimate parent values (\hat{t}, \hat{i}) from a counterfactual image x generated by learned model $p(x | t, i)$

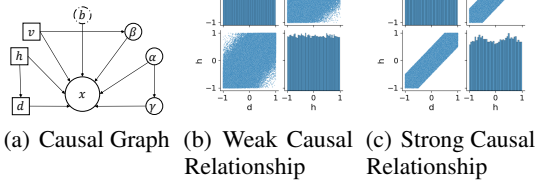
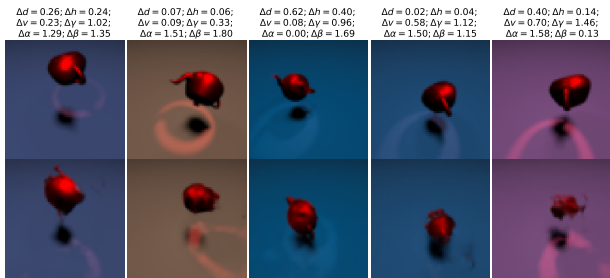
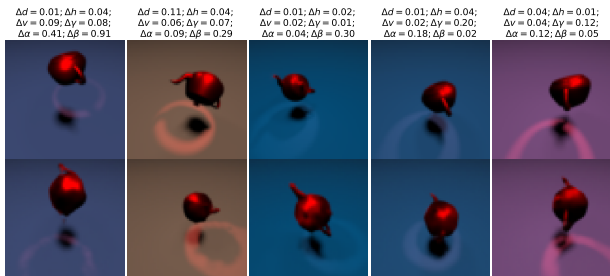


Figure 4. Causal graph of 3DIdent and the causal relationships of variables (d, h) in Weak-3DIdent and Strong-3DIdent respectively.



(a) Results of Non-backtracking Counterfactuals



(b) Results of Natural Counterfactuals

Figure 5. Visualization Results on Strong-3DIdent (View the enlarged figure in Fig. 10 in the Appendix).

with the input (t, i) , and then computing the absolute error $|t - \hat{t}|$ or $|i - \hat{i}|$ between the input (t, i) and their predicted counterparts (\hat{t}, \hat{i}) as inferred from counterfactual images.

Ablation Study on Naturalness Threshold ϵ . Table 2 demonstrates that our error decreases with increasing ϵ , regardless of whether V-SCM or H-SCM is used. This trend suggests that a larger ϵ sets a stricter standard for naturalness in counterfactuals, enhancing the feasibility of interventions and consequently lowering prediction errors. This improvement is likely because deep-learning models are more adept at generalizing to high-frequency data (Engstrom et al., 2019).

Table 3. Results on Weak-3DIdent and Strong-3DIdent (abbreviated as “Weak” “Strong” for simplicity). For clarity, we use “Non” to denote Nonbacktracking.

Dataset	-	d	h	v	γ	α	β	b
Weak	Non	0.025	0.019	0.035	0.364	0.27	0.077	0.0042
	Ours	0.024	0.018	0.034	0.349	0.221	0.036	0.0041
Strong	Non	0.100	0.083	0.075	0.387	0.495	0.338	0.0048
	Ours	0.058	0.047	0.050	0.298	0.316	0.139	0.0047

6.3. 3DIdentBOX

In this study, we employ two practical public datasets from 3DIdentBOX (Bizeul et al., 2023), namely Weak-3DIdent and Strong-3DIdent. Both datasets share the same causal graph, as depicted in Fig. 4 (a), which includes an image variable x and its seven parent variables, with three pairs of parent variables: (h, d) , (v, β) , and (α, γ) , where one is the direct cause of the other in each pair. The primary distinction between Weak-3DIdent and Strong-3DIdent lies in the strength of the causal relationships between each variable pair, with Weak-3DIdent exhibiting weaker connections (Fig. 4 (b)) compared to Strong-3DIdent (Fig. 4 (c)). Our approach mirrors the MorphoMNIST experiments, using H-SCM as the learned SCM with $\epsilon = 10^{-3}$.

Influence of Causal Effect Strength. As Table 3 reveals, our method outperforms non-backtracking on both datasets, with a notably larger margin in Strong-3DIdent. This increased superiority is due to a higher incidence of infeasible hard interventions in non-backtracking counterfactuals within the Strong-3DIdent dataset.

Visualization on Strong-3DIdent. Fig. 5 displays counterfactuals, with the text above the evidence images (first row) indicating errors for the counterfactual images (second row). In Fig. 5 (a), it is evident that some images (second, third and fifth images in particular), generated by non-backtracking counterfactuals are less recognizable and have larger errors. Conversely, our counterfactual images exhibit better visual clarity and more distinct shapes, as our natural counterfactuals consistently ensure feasible interventions, resulting in more natural-looking images.

See Appendix for More Details. For in-depth information on datasets, experimental results’ standard deviation, model training settings, Feasible Intervention Optimization, differences between our natural counterfactuals and related works, and mechanism distance for natural counterfactuals, refer to the Appendix.

7. Conclusion

To address the impractical scenarios often generated by non-backtracking counterfactuals, we introduces natural counterfactuals. This concept emphasizes real-world applicability by determining feasible intervention, thereby aligning counterfactuals with the data distribution of the actual world. By integrating a naturalness constraint with necessary backtracking, we have developed an optimization framework designed to determine feasible interventions. This method has been effectively demonstrated through various deep learning case studies, highlighting its capability to yield more dependable and precise counterfactuals. Future work involving natural counterfactuals could focus on exploring their applicability and impact in crucial areas like explainable AI and healthcare.

References

- Ash, R. B. *Information theory*. Courier Corporation, 2012.
- Barocas, S., Selbst, A. D., and Raghavan, M. The hidden assumptions behind counterfactual explanations and principal reasons. In *FAT*, 2020.
- Bizeul, A., Daunhawer, I., Palumbo, E., Schölkopf, B., Marx, A., and Vogt, J. E. 3didentbox: A toolbox for identifiability benchmarking. 2023.
- Boyd, S. P. and Vandenberghe, L. *Convex optimization*. Cambridge university press, 2004.
- Castro, D. C., Tan, J., Kainz, B., Konukoglu, E., and Glocker, B. Morpho-mnist: quantitative assessment and diagnostics for representation learning. *Journal of Machine Learning Research*, 20(178):1–29, 2019.
- Conde, M. R. Necessity defined: A new role in the criminal defense system. *UCLA L. Rev.*, 29:409, 1981.
- Dash, S., Balasubramanian, V. N., and Sharma, A. Evaluating and mitigating bias in image classifiers: A causal perspective using counterfactuals. In *Proceedings of the IEEE/CVF Winter Conference on Applications of Computer Vision*, pp. 915–924, 2022.
- Dehghani, M., Iliev, R., and Kaufmann, S. Causal explanation and fact mutability in counterfactual reasoning. *Mind & Language*, 27(1):55–85, 2012.
- Dhurandhar, A., Chen, P.-Y., Luss, R., Tu, C.-C., Ting, P., Shanmugam, K., and Das, P. Explanations based on the missing: Towards contrastive explanations with pertinent negatives. In *NeurIPS*, 2018.
- Engstrom, L., Ilyas, A., Salman, H., Santurkar, S., and Tsipras, D. Robustness (python library), 2019. URL <https://github.com/MadryLab/robustness>. License: MIT.
- Gerstenberg, T., Bechlvaniadis, C., and Lagnado, D. A. Back on track: Backtracking in counterfactual reasoning. In *Proceedings of the Annual Meeting of the Cognitive Science Society*, volume 35, 2013.
- Hassanpour, N. and Greiner, R. Learning disentangled representations for counterfactual regression. In *International Conference on Learning Representations*, 2019.
- Hiddleston, E. A causal theory of counterfactuals. *Noûs*, 39(4):632–657, 2005.
- Kingma, D. and Welling, M. Auto-encoding variational bayes. In *ICLR*, 2014.
- Kocaoglu, M., Snyder, C., Dimakis, A. G., and Vishwanath, S. Causalgan: Learning causal implicit generative models with adversarial training. In *International Conference on Learning Representations*.
- Lewis, D. Counterfactual dependence and time’s arrow. *Noûs*, pp. 455–476, 1979.
- Loshchilov, I. and Hutter, F. Decoupled weight decay regularization. In *International Conference on Learning Representations*, 2018.
- Lu, C., Huang, B., Wang, K., Hernández-Lobato, J. M., Zhang, K., and Schölkopf, B. Sample-efficient reinforcement learning via counterfactual-based data augmentation. *arXiv preprint arXiv:2012.09092*, 2020.
- Maaløe, L., Fraccaro, M., Liévin, V., and Winther, O. Biva: A very deep hierarchy of latent variables for generative modeling. *Advances in neural information processing systems*, 32, 2019.
- Monteiro, M., Ribeiro, F. D. S., Pawlowski, N., Castro, D. C., and Glocker, B. Measuring axiomatic soundness of counterfactual image models. *arXiv preprint arXiv:2303.01274*, 2023.
- Mothilal, R. K., Sharma, A., and Tan, C. Explaining machine learning classifiers through diverse counterfactual explanations. In *FAccT*, 2020.
- Oberst, M. and Sontag, D. Counterfactual off-policy evaluation with gumbel-max structural causal models. In *International Conference on Machine Learning*, pp. 4881–4890. PMLR, 2019.
- Pawlowski, N., Coelho de Castro, D., and Glocker, B. Deep structural causal models for tractable counterfactual inference. *Advances in Neural Information Processing Systems*, 33:857–869, 2020.
- Pearl, J. *Causality*. Cambridge university press, 2009.
- Ribeiro, F. D. S., Xia, T., Monteiro, M., Pawlowski, N., and Glocker, B. High fidelity image counterfactuals with probabilistic causal models. 2023.
- Sanchez, P. and Tsafaris, S. A. Diffusion causal models for counterfactual estimation. In *First Conference on Causal Learning and Reasoning*.
- Schölkopf, B., Locatello, F., Bauer, S., Ke, N. R., Kalchbrenner, N., Goyal, A., and Bengio, Y. Toward causal representation learning. *Proceedings of the IEEE*, 109(5): 612–634, 2021.
- Schut, L., Key, O., McGrath, R., Costabello, L., Sacaleanu, B., Corcoran, M., and Gal, Y. Generating interpretable counterfactual explanations by implicit minimisation of epistemic and aleatoric uncertainties. In *AISTATS*, 2021.

Verma, S., Dickerson, J. P., and Hines, K. Counterfactual explanations for machine learning: A review. *arXiv preprint, arXiv:2010.10596*, 2020.

von Kügelgen, J., Mohamed, A., and Beckers, S. Backtracking counterfactuals. *arXiv preprint arXiv:2211.00472*, 2022.

Wachter, S., Mittelstadt, B., and Russell, C. Counterfactual explanations without opening the black box: Automated decisions and the GDPR. *Harvard Journal of Law & Technology*, 2018.

A. Datasets and More Experimental Results

In this section, we first provide detailed datasets settings and additional experimental results. Subsequently, we present the standard deviation of all experimental outcomes in Sec. A.

A.1. Toy Datasets

We design four simulation datasets, *Toy 1-4*, and use the designed SCMs to generate 10,000 data points as a training dataset and another 10,000 data points as a test set for each dataset. Fig. 6 shows causal graphs of *Toy 1-4* and scatter plot matrices of test datasets in each dataset. The ground-truth SCMs of each dataset are listed below.

Toy 1.

$$\begin{aligned} n_1 &= u_1, & u_1 &\sim \mathcal{N}(0, 1), \\ n_2 &= -n_1 + \frac{1}{3}u_2, & u_2 &\sim \mathcal{N}(0, 1), \\ n_3 &= \sin [0.25\pi(0.5n_2 + n_1)] + 0.2u_3, & u_3 &\sim \mathcal{N}(0, 1), \end{aligned}$$

where there are three endogenous variables (n_1, n_2, n_3) and three noise variables (u_1, u_2, u_3) . n_1 is the confounder of n_2 and n_3 and n_1 and n_2 causes n_3 .

Toy 2.

$$\begin{aligned} n_1 &= u_1, & u_1 &\sim \mathcal{N}(0, 1), \\ n_2 &= \sin [0.2\pi(n_2 + 2.5)] + 0.2u_2, & u_2 &\sim \mathcal{N}(0, 1), \end{aligned}$$

where there are three endogenous variables (n_1, n_2) and three noise variables (u_1, u_2) . n_1 causes n_2 .

Toy 3.

$$\begin{aligned} n_1 &= u_1, & u_1 &\sim \mathcal{N}(0, 1), \\ n_2 &= -n_1 + \frac{1}{3}u_2, & u_2 &\sim \mathcal{N}(0, 1), \\ n_3 &= \sin [0.1\pi(n_2 + 2.0)] + 0.2u_3, & u_3 &\sim \mathcal{N}(0, 1), \\ n_4 &= \sin [0.25\pi(n_3 - n_1 + 2.0)] + 0.2u_4, & u_4 &\sim \mathcal{N}(0, 1), \end{aligned}$$

where there are three endogenous variables (n_1, n_2, n_3, n_4) and three noise variables (u_1, u_2, u_3, u_4) . n_1 is the confounder of n_1 and n_4 . (n_2, n_3, n_4) is a chain, i.e., n_2 causes n_3 , followed by n_4 .

Toy 4.

$$\begin{aligned} n_1 &= u_1, & u_1 &\sim \mathcal{N}(0, 1), \\ n_2 &= -n_1 + \frac{1}{3}u_2, & u_2 &\sim \mathcal{N}(0, 1), \\ n_3 &= \sin [0.3\pi(n_2 + 2.0)] + 0.2u_3, & u_3 &\sim \mathcal{N}(0, 1), \end{aligned}$$

where there are three endogenous variables (n_1, n_2, n_3) and three noise variables (u_1, u_2, u_3) . (n_1, n_2, n_3) is a chain, i.e., n_1 causes n_2 , followed by n_3 .

Table 4. MAE Results on Toy 1 – 4. For simplicity, we use *do* operator in the table to save room, and when natural counterfactuals are referred to, *do* means *change*.

Dataset	<i>Toy 1</i>			<i>Toy 2</i>			<i>Toy 3</i>				<i>Toy 4</i>		
<i>do</i> or <i>change</i>	do(n_1)	do(n_2)	do(n_3)	do(n_1)	do(n_2)	do(n_3)	do(n_1)	do(n_2)	do(n_3)	do(n_4)	do(n_1)	do(n_2)	do(n_3)
Outcome	n_2	n_3	n_3	n_2	n_2	n_3	n_4	n_3	n_4	n_4	n_2	n_3	n_3
Nonbacktracking	0.477	0.382	0.297	0.315	0.488	0.472	0.436	0.488	0.230	0.179	0.166	0.446	0.429
Ours	0.434	0.354	0.114	0.303	0.443	0.451	0.423	0.127	0.136	0.137	0.158	0.443	0.327

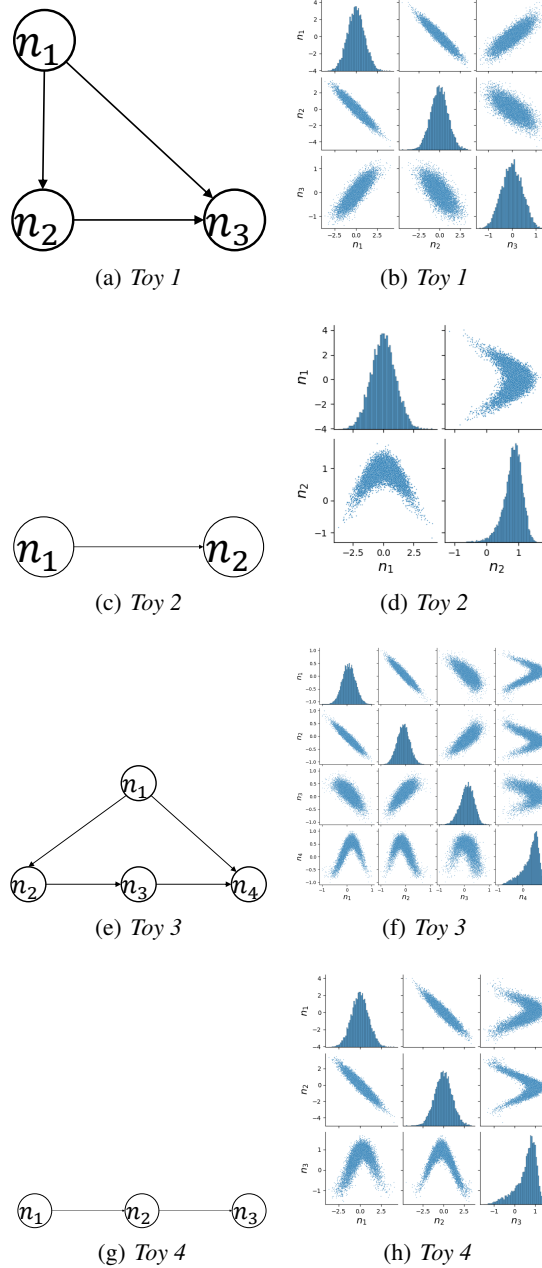


Figure 6. Causal graphs and Scatter Plot Matrices of *Toy 1-4*. Figure (a) (c) (e) and (g) show causal graphs of *Toy 1-4* respectively. Figure (b) (d) (f) and (h) indicate scatter plot matrices of variables in *Toy 1-4* respectively.

In the main paper, we have explain experiments on *Toy 1* in details. As shown in Table 4, our performance on *Toy 2-4* shows big margin compared with non-backtracking counterfactuals since natural counterfactuals consistently make interventions feasible, while part of hard interventions may not be feasible in non-backtracking counterfactuals.

Visualization Results on *Toy 1*. In Fig. 7, larger counterfactual images are displayed, which are identical to those shown in Fig. 2, with the only difference being their size.

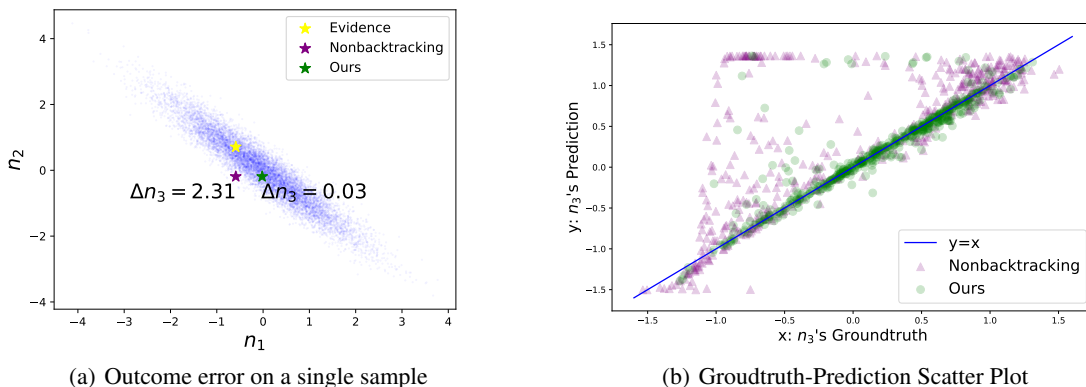


Figure 7. The Visualization Results on *Toy 1*.

A.2. MorphoMNIST

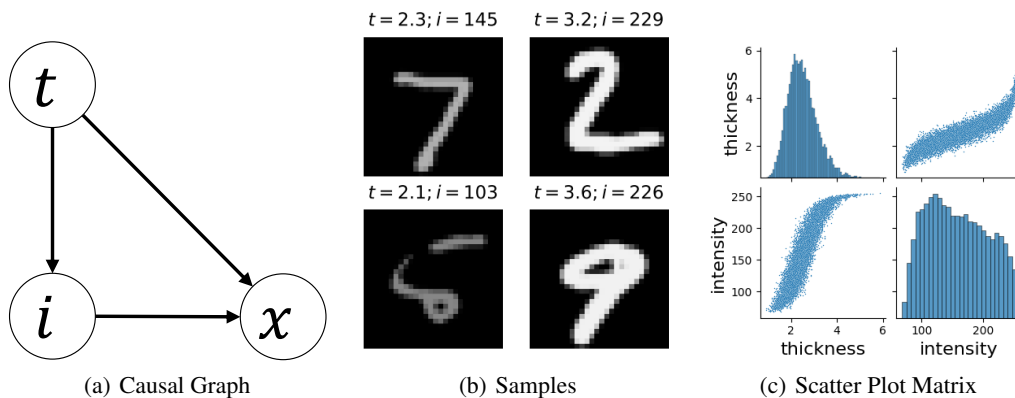


Figure 8. Causal Graph and samples of Morpho-MNIST.

The MorphoMNIST comes from (Pawlowski et al., 2020), where there are 60000 images as training set and 10,000 images as test dataset. Fig. 8 (a) shows the causal graph for generating Morpho-MNIST; specifically, stroke thickness t causes the brightness intensity i , and both thickness t and intensity i cause the digit x . Fig. 8 (b) show some samples from Morpho-MNIST. The ground-truth SCMs to generate the Morpho-MNIST are as follows:

$$\begin{aligned}
 t &= 0.5 + u_t, & u_t &\sim \Gamma(10, 5), \\
 i &= 191 \cdot \sigma(0.5 \cdot u_i + 2 \cdot t - 5) + 64, & u_i &\sim \mathcal{N}(0, 1), \\
 x &= \text{SetIntensity}(\text{SetThickness}(u_x; t); i), & u_x &\sim \text{MNIST},
 \end{aligned}$$

where u_t , u_i , and u_x are noise variables, and σ is the sigmoid function. $\text{SetThickness}(\cdot; t)$ and $\text{SetIntensity}(\cdot; i)$ are the operations to set an MNIST digit u_x 's thickness and intensity to i and t respectively, and x is the generated image.

Quantitative Results of $\text{change}(i)$ or $\text{do}(i)$. We use V-SCM to do counterfactual task of $\text{change}(i)$ (where $\epsilon = 10^{-3}$) or $\text{do}(i)$ with multiple random seeds on test set. In Table 5, the first column shows the MAE of (t, i) , indicating our results outperform that of non-backtracking, since our approach consistently determine feasible interventions.

Table 5. MorphoMNIST results of $change(i)$ or $do(i)$ using V-SCM

Intersection between Ours and NB			(NCO=1, NB=1)	(NCO=1, NB=0)	(NCO=0, NB=1)	(NCO=0, NB=0)
Number of Intersection			5865	3159	0	975
Nonbacktracking	t 's MAE	0.283	0.159	0.460	0.000	0.450
	i 's MAE	6.56	3.97	8.95	0.000	14.3
Ours	t 's MAE	0.164	0.160	0.171	0.000	0.466
	i 's MAE	4.18	4.01	4.49	0.000	14.1

The Effectiveness of Feasible Intervention Optimization (FIO). Next, we focus on the rest four-column results. In both types of counterfactuals, we use the same value i in $do(i)$ and $change(i)$. Hence, after inference, we know which image satisfies ϵ -natural generation in the two types of counterfactuals. In "NC=1" of the table, NC indicates the set of counterfactuals after feasible intervention optimization. Notice that NC set does not mean the results of natural counterfactuals, since some results do still not satisfy ϵ -natural generation after FIO. "NC=1" mean the set containing data points satisfying ϵ -natural generation and "NC=0" contains data not satisfying ϵ -natural generation after feasible intervention optimization. Similarly, "NB=1" means the set containing data points satisfying naturalness criteria. (NC=1, NB=1) presents the intersection of "NC=1" and "NB=1". Similar logic is adopted to the other three combinations. The number of counterfactual data points are 10, 000 in two types of counterfactuals.

In (NC=1, NB=1) containing 5865 data points, our performance is similar to the non-backtracking, showing feasible intervention optimization tends to backtrack as less as possible when hard interventions have satisfied ϵ -natural generation. In (NC=1, NB=0), there are 3159 data points, which are "unnatural" points in non-backtracking counterfactuals. After natural counterfactual optimization, this huge amount of data points becomes "natural". Here, our approach significantly reduces errors, achieving a 62.8% reduction in thickness t and 49.8% in intensity i , the most substantial improvement among the four sets in Table 5. The number of points in (NC=0, NB=1) is zero, showing the stability of our algorithm since our FIO framework will change the hard, feasible intervention into unfeasible intervention. Two types of counterfactuals perform similarly in the set (NC=0, NB=0), also showing the stability of our approach.

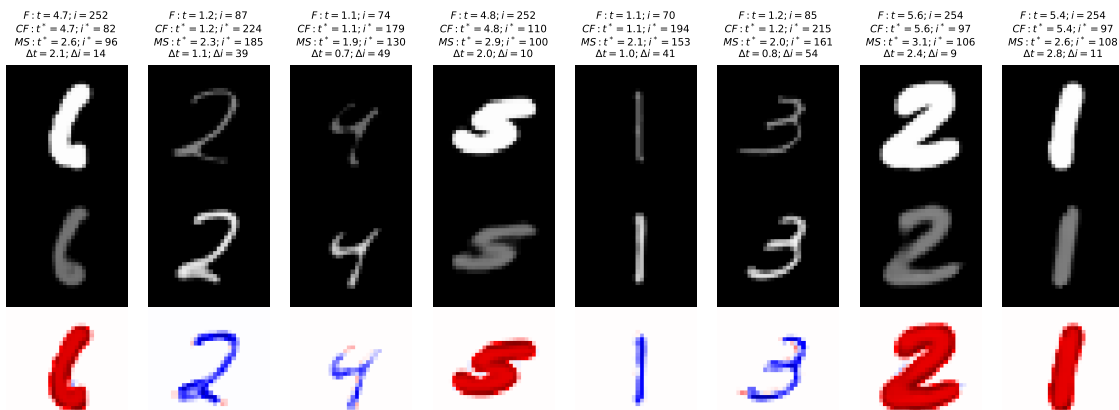
Visualization of Counterfactual Images. Fig. 9 shows counterfactual images (second row), based on the evidence images (first row), with intended changes on i . The third row illustrates the differences between evidence and counterfactual images. Focusing on the first counterfactual image from non-backtracking and natural counterfactuals respectively, in non-backtracking, despite $do(i)$ where thickness value 4.2 should remain unchanged, the counterfactual image shows reduced thickness, consistent with the measured counterfactual thickness of 2.6. In contrast, natural counterfactuals yield an estimated counterfactual thickness (t^* in MS) closely matching original counterfactual thickness (t^* in CF), due to backtracking for a feasible intervention on the earlier causal variable t , thereby maintaining (t, i) within the data distribution. Observing other images also shows larger errors in non-backtracking counterfactual images.

A.3. 3DIdentBOX

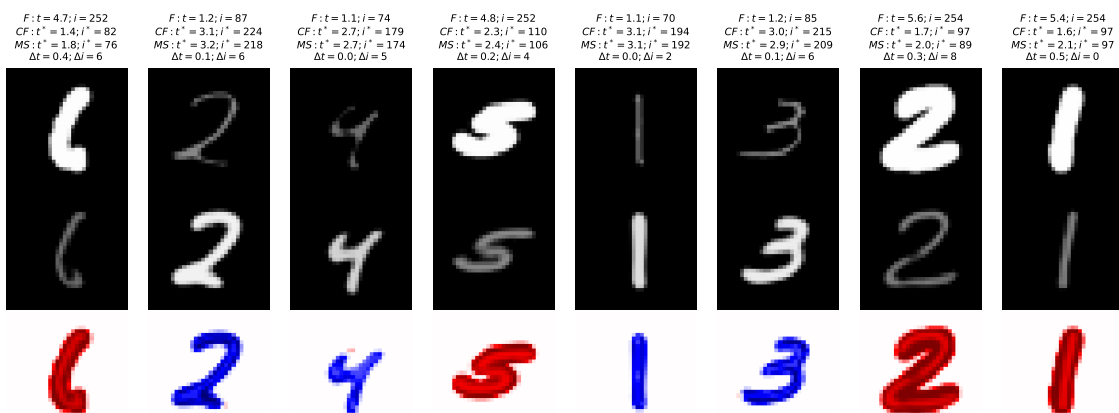
Table 6. Details of variables in 3DIdentBOX. Object refers to teapot in each image. The support of each variable is $[-1, 1]$. The real visual range are listed in the column **Visual Range**.

Information Block	Variables	Support	Description	Visual Range
Position	x	$[-1, 1]$	Object x-coordinate	-
	y	$[-1, 1]$	Object y-coordinate	-
	z	$[-1, 1]$	Object z-coordinate	-
Rotation	γ	$[-1, 1]$	Spotlight rotation angle	$[0^\circ, 360^\circ]$
	α	$[-1, 1]$	Object α -rotation angle	$[0^\circ, 360^\circ]$
	β	$[-1, 1]$	Object β -rotation angle	$[0^\circ, 360^\circ]$
Hue	b	$[-1, 1]$	Background HSV color	$[0^\circ, 360^\circ]$

The 3DIdentBOX datasets, first introduced in Bizeul et al. (2023), come with official code for generating customized versions of these datasets. They consist of images created with Blender, each depicting a teapot with seven attributes, such as position, rotation, and hue, determined by seven ground-truth variables.



(a) Results of Non-backtracking Counterfactuals



(b) Results of Natural Counterfactuals

Figure 9. Visualization Results on MorphoMNIST: “F” stands for factual values, “CF” for counterfactual values, and “MS” for estimated counterfactual values of (t, i) . $(\Delta t, \Delta i)$ represents the absolute errors between counterfactual and estimated counterfactual values of (t, i) .

In our experiment with the 3DIdentBOX, which comprises six datasets, we focus on the *positions-rotations-hue* dataset. We expand this into two datasets, Weak-3DIdent and Strong-3DIdent. Each dataset includes seven variables, besides the image variable x , with specifics outlined in Table 6. Every image features a teapot, with variables categorized into three groups: positions (x, y, z) , rotations (γ, α, β) , and hue b , representing seven teapot attributes, as depicted in 11 (a). Fig. 11 (b) illustrates that both datasets share the same causal graph. The distributions of several parent variables of image x in these datasets are detailed in Table 7.

Visualization on Strong-3DIdent. In Fig. 10, larger counterfactual images are displayed, which are identical to those shown in Fig. 5, with the only difference being their size.

A.4. Standard Deviation of Experimental Results

This section presents the standard deviation of all experimental results, demonstrating that the standard deviation for our natural counterfactuals is generally lower. This indicates the increased reliability of our approach, achieved by necessary backtracking to ensure counterfactuals remain within data distributions.

Natural Counterfactuals With Necessary Backtracking

Table 7. Distributions in Weak-3DIdent and Strong-3DIdent. $\mathcal{N}_{wt}(y, 1)$ refers to a normal distribution truncated to the interval $[-1, 1]$ and $\mathcal{N}_{st}(y, 1)$ means a normal distribution truncated to the interval $[\min(1, y + 0.2), \max(-1, y - 0.2)]$, where min and max indicate operations that select smaller and bigger values respectively. $\mathcal{N}_{wt}(\alpha, 1)$ and $\mathcal{N}_{st}(\alpha, 1)$ are identical to $\mathcal{N}_{wt}(y, 1)$ and $\mathcal{N}_{st}(y, 1)$ respectively. U refers to uniform distribution.

Variables	Weak-3DIdent Distribution	Strong-3DIdent Distribution
$c = (x, y, z)$	$c \sim (\mathcal{N}_{wt}(y, 1), U(-1, 1), U(-1, 1))$	$c \sim (\mathcal{N}_{st}(y, 1), U(-1, 1), U(-1, 1))$
$s = (\gamma, \alpha, \beta)$	$s \sim (\mathcal{N}_{wt}(\alpha, 1), U(-1, 1), \mathcal{N}_{wt}(z, 1))$	$s \sim (\mathcal{N}_{st}(\alpha, 1), U(-1, 1), \mathcal{N}_{st}(z, 1))$
b	$b \sim U(-1, 1)$	$b \sim U(-1, 1)$

Table 8. Standard Deviation of Results on Toy 1 – 4.

Dataset	Toy 1		Toy 2		Toy 3				Toy 4				
<i>do</i> or <i>change</i>	<i>do</i> (n_1)		<i>do</i> (n_2)	<i>do</i> (n_1)	<i>do</i> (n_1)		<i>do</i> (n_2)	<i>do</i> (n_3)	<i>do</i> (n_1)	<i>do</i> (n_2)			
Outcome	n_2	n_3	n_3	n_2	n_2	n_3	n_4	n_3	n_4	n_4	n_2	n_3	n_3
Nonbacktracking	0.00184	0.00628	0.00432	0.00164	0.00448	0.00686	0.00495	0.0112	0.00556	0.00142	0.000514	0.00623	0.00238
Ours	0.00409	0.00684	0.00295	0.00191	0.00116	0.00461	0.00201	0.00504	0.00531	0.00155	0.000235	0.00518	0.00143

Table 9. Standard Deviation of Results on MorphoMNIST

Intersection between Ours and NB Number of Intersection			(NCO=1, NB=1)	(NCO=1, NB=0)	(NCO=0, NB=1)	(NCO=0, NB=0)
			39.84	81.43	0.00	54.14
Nonbacktracking	t 's MAE	0.00322	0.00172	0.00670	0.000	0.0178
	i 's MAE	0.0496	0.0596	0.0508	0.000	0.110
Ours	t 's MAE	0.00137	0.00222	0.00157	0.000	0.0149
	i 's MAE	0.0359	0.0551	0.0157	0.000	0.0853

Table 10. Standard Deviation of Ablation Study on ϵ

Model	ϵ	CFs	<i>do</i> (t)		<i>do</i> (i)	
			t	i	t	i
V-SCM	-	NB	0.000512	0.0172	0.00322	0.0496
	10^{-4}	Ours	0.00159	0.0210	0.00183	0.0561
	10^{-3}		0.00124	0.0217	0.00137	0.0359
	10^{-2}		0.000954	0.0382	0.000868	0.0556
H-SCM	-	NB	0.000915	0.0229	0.000832	0.0245
	10^{-4}	Ours	0.000920	0.0178	0.000922	0.0138
	10^{-3}		0.000611	0.0206	0.000289	0.0264
	10^{-2}		0.000787	0.0244	0.000431	0.0258

Table 11. Standard Deviation of Results on Weak-3DIdent and Strong-3DIdent

Dataset	Counterfactuals	d	h	v	γ	α	β	b
Weak-3DIdent	Nonbacktracking	3.68e-05	0.000133	0.000226	0.00422	0.00310	0.00357	1.29e-05
	Ours	4.27e-05	7.22e-05	0.000249	0.00558	0.00278	0.00136	3.33e-05
Strong-3DIdent	Nonbacktracking	0.00233	0.000864	0.00127	0.00933	0.00307	0.00452	1.49e-05
	Ours	0.00166	0.000774	0.000229	0.00908	0.00955	0.00816	2.97e-05

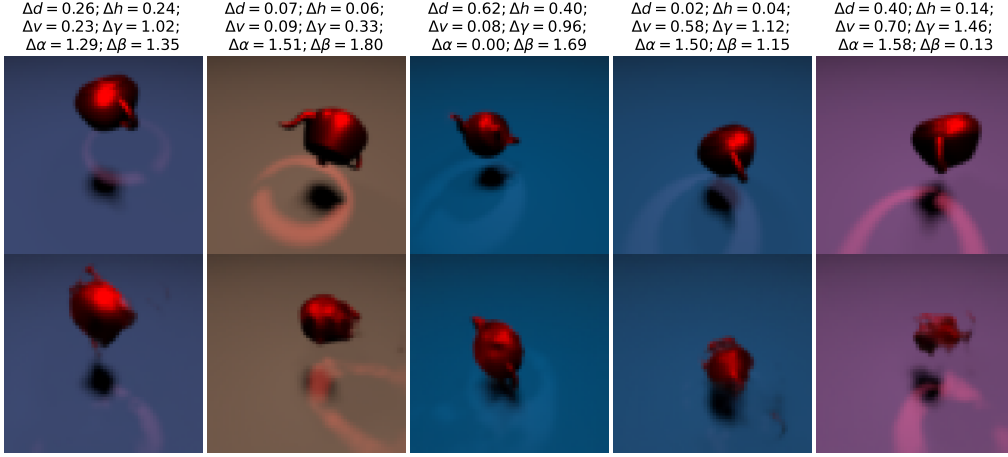
B. Proof for Theorem 4.1

Theorem 1 from Lu et al. (2020) details identifiable counterfactuals under a certain condition:

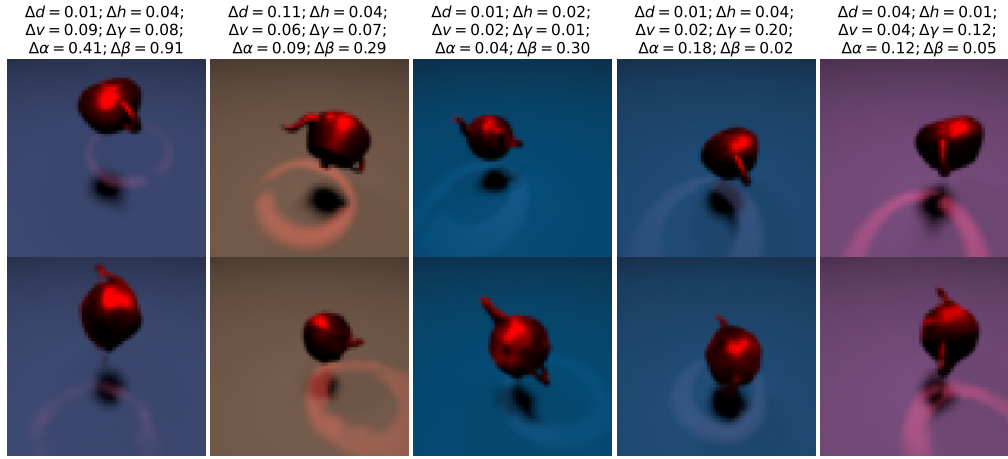
Theorem B.1 (Identifiable Counterfactuals). *Suppose \mathbf{V}_i satisfies the following structural causal model:*

$$\mathbf{V}_i := f_i(\mathbf{PA}_i, \mathbf{U}_i)$$

Natural Counterfactuals With Necessary Backtracking



(a) Results of Non-backtracking Counterfactuals



(b) Results of Natural Counterfactuals

Figure 10. Visualization Results on Stong-3DIdent.

where $\mathbf{U}_i \perp \mathbf{PA}_i$ and assume unknown f_i is smooth and strictly monotonic w.r.t. \mathbf{U}_i for fixed values of \mathbf{PA}_i . If we have observed $\mathbf{V}_i = \mathbf{v}_i$ and $\mathbf{PA}_i = pa_i$, with an intervention $do(\mathbf{PA}_i = pa_i^*)$, the counterfactual outcome is identifiable:

$$\mathbf{V}_i | do(\mathbf{PA}_i = pa_i^*), \mathbf{V}_i = \mathbf{v}_i, \mathbf{PA}_i = pa_i \quad (6)$$

We use this theorem to support our proof for Theorem 4.1, which extends Theorem B.1 to a broader range of identifiable counterfactuals.

Proof. We initially assume the presence of complete evidence, meaning $\mathbf{E} = \mathbf{V}$. In line with Theorem B.1 from (Lu et al., 2020), counterfactual outcome of $\mathbf{B}_k \in \mathbf{B}$ is identifiable when given the counterfactual action $\mathbf{PA}_{\mathbf{B}_k} = pa_{\mathbf{B}_k}^*$, alongside the observable values $\mathbf{B}_k = \mathbf{b}_k$ and $\mathbf{PA}_{\mathbf{B}_k} = pa_{\mathbf{B}_k}$, where \mathbf{B}_k is any variable in \mathbf{B} and $\mathbf{PA}_{\mathbf{B}_k}$ is the parent set of \mathbf{B}_k .

With this full evidence assumption, $pa_{\mathbf{B}_k}^*$ is conclusively determined by the complete evidence and the intervention $do(\mathbf{C} = \mathbf{c}^*)$, whereas $pa_{\mathbf{B}_k}$ and $\mathbf{B}_k = \mathbf{b}_k$ are ascertained from the full evidence. This ensures the counterfactual outcome of \mathbf{B}_k , a single value, is identifiable. Extending this logic, the counterfactual outcome of \mathbf{B} as a whole, also a single value, is identifiable. Consequently, $p(\mathbf{B} | do(\mathbf{C} = \mathbf{c}^*), \mathbf{E} = \mathbf{e})$ is identifiable with a singular value as its support.

Next, we consider the case of partial evidence, where $\mathbf{E} \subset \mathbf{V}$. Given that $p(\mathbf{B} | do(\mathbf{C} = \mathbf{c}^*), \mathbf{E} = \mathbf{e}) = \int p(\mathbf{B} | \mathbf{V} = \mathbf{v}, do(\mathbf{C} = \mathbf{c}^*)) p(\mathbf{V} = \mathbf{v} | \mathbf{E} = \mathbf{e}) d\mathbf{V}$ and both terms $p(\mathbf{B} | \mathbf{V} = \mathbf{v}, do(\mathbf{C} = \mathbf{c}^*))$ (treat $\mathbf{V} = \mathbf{v}$ as full evidence) and $p(\mathbf{V} = \mathbf{v} | \mathbf{E} = \mathbf{e})$ are identifiable, it follows that $p(\mathbf{B} | do(\mathbf{C} = \mathbf{c}^*), \mathbf{E} = \mathbf{e})$ is also identifiable. □

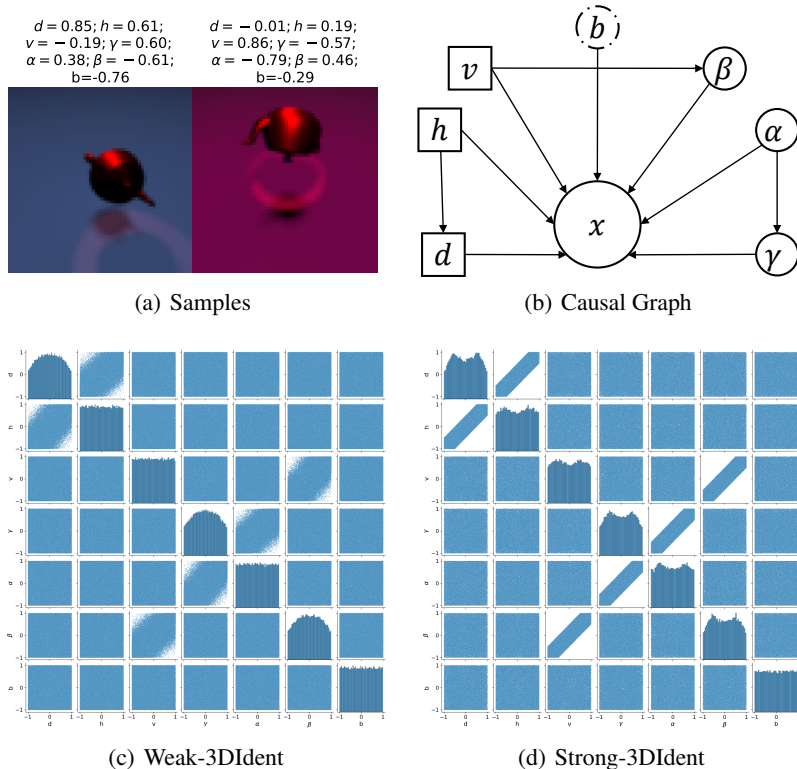


Figure 11. Samples, Causal Graph, Scatter Plot Matrices of Weak-3DIdent and Strong-3DIdent.

C. Model Training

Our study focuses on counterfactual inference and we directly use two state-of-the-art deep-learning SCM models to learn SCMs among variables using a dataset, i.e., D-SCM (Pawłowski et al., 2020) and H-SCM (Ribeiro et al., 2023). Specifically, we use code of (Ribeiro et al., 2023) containing the implementation of D-SCM and H-SCM. Take Morpho-MNIST as an example, in both two models, normalizing flows are firstly trained to learn causal mechanisms for all variables except image x , i.e., (t, i) , and a conditional VAE is used to model image x given its parents (t, i) . For D-SCM, the conditional VAE uses normal VAE framework, while H-SCM uses hierarchical VAE structure (Maaløe et al., 2019) to better capture the distribution of images.

Toy Experiments. In the case of four toy experiments, we exclusively employed normalizing flows due to the fact that all variables are one-dimensional. Our training regimen for the flow-based model spanned 2000 epochs, utilizing a batch size of 100 in conjunction with the AdamW optimizer (Loshchilov & Hutter, 2018). We initialized the learning rate to 1×10^{-3} , set β_1 to 0.9, β_2 to 0.9.

MorphoMNIST. We first train normalized flows to learn causal mechanisms of thickness and intensity (t, i) . Other hyper-parameters are similar to those of toy experiments. Then, we train two VAE-based models (D-SCM and H-SCM) to learn x given (t, i) respectively. The architectures of the two models are identical to (Ribeiro et al., 2023). D-SCM and H-SCM underwent training for 160 epochs. We employed a batch size of 32 and utilized the AdamW optimizer. The initial learning rate was set to $1e-3$ and underwent a linear warmup consisting of 100 steps. We set β_1 to 0.9, β_2 to 0.9, and applied a weight decay of 0.01. Furthermore, we implemented gradient clipping at a threshold of 350 and introduced a gradient update skipping mechanism, with a threshold set at 500 based on the L^2 norm. During the testing, i.e., counterfactual inference, we test performance on both models respectively, with the normalized flows.

3DIdentBOX. Similar to experiments on MorphoMNIST, we first train normalized flows. Compared with D-SCM, H-SCM is more powerful to model complex data like 3DIdentBOX, of which the size of the image is $64 \times 64 \times 4$. Then, we train H-SCM to capture the distribution of x given its parents for 500 epochs with a batch size of 32. The hyper-parameters are the same as experiments on MorphoMNIST.

D. Feasible Intervention Optimization

Our loss function for Feasible Intervention Optimization is defined as:

$$\mathcal{L} = \|an(\mathbf{A}) - an(\mathbf{A})^*\|_1 + w_\epsilon \sum_j [\max(\epsilon - F(\mathbf{V}_j = \mathbf{v}_j^* | pa_j^*), 0) + \max(\epsilon + F(\mathbf{V}_j = \mathbf{v}_j^* | pa_j^*) - 1, 0)]$$

$$s.t. \quad \mathbf{A} = \mathbf{a}^*$$
(7)

Based on Theorem 4.1, Choice (3) of naturalness constraints is equivalent to Choice (2), as $F(\mathbf{V}_j = \mathbf{v}_j^* | pa_j^*) = F(\mathbf{U}_j = \mathbf{u}_j^*)$ with $\mathbf{v}_j^* = f_j(pa_j^*, \mathbf{u}_j^*)$. Hence, the loss can be rewritten as:

$$\mathcal{L} = \|an(\mathbf{A}) - an(\mathbf{A})^*\|_1 + w_\epsilon \sum_j [\max(\epsilon - F(\mathbf{u}_j^*), 0) + \max(\epsilon + F(\mathbf{u}_j^*) - 1, 0)]$$

$$s.t. \quad \mathbf{u}_A^* = f_A^{-1}(\mathbf{a}^*, \mathbf{pa}_A^*)$$
(8)

Note that \mathbf{u}_A is not explicitly optimized as its value, \mathbf{pa}_A , is determined by other noise values and the constant \mathbf{a}^* through the reversible function f_A^{-1} . Consequently, \mathbf{u}_A is indirectly determined by other noise values and \mathbf{a}^* . The loss's parameter is thus \mathbf{u}_{AN}^* , which fully determines the value $an(\mathbf{A})^*$ using the learned SCM, as explained in Sec. C.

In all experiments, we optimized \mathbf{u}_{AN}^* using the AdamW optimizer at a learning rate of $1e - 3$ for 50,000 steps. This approach's effectiveness is validated by the MorphoMNIST experiments.

E. Standard Procedure of Natural Counterfactuals

In this section, we outline our natural counterfactuals' standard procedure, assuming full evidence. Through Feasible Intervention Optimization, we obtain the optimal value $an(\mathbf{A})^*$. This identifies the changed variables, \mathbf{C} , which we target for intervention, enabling the definition of the feasible intervention $do(\mathbf{C} = \mathbf{c}^*)$, with \mathbf{c}^* as the post-optimization counterfactual values of \mathbf{C} . Then, we can do natural counterfactuals given the feasible intervention $do(\mathbf{C} = \mathbf{c}^*)$. Accordingly, we provide a three-step standard procedure for our general natural counterfactuals:

Theorem E.1 (Natural Counterfactuals). *With the model $\langle \mathcal{M}, p(\mathbf{U}) \rangle$ and ϵ , the probability $p(\mathbf{B}_A | \mathbf{e})$ of a counterfactual condition "Given the evidence $\mathbf{E} = \mathbf{e}$, if \mathbf{A} 's value is changed into \mathbf{a}^* due to the feasible interventions on causally earlier variables, then \mathbf{B} ," can be predicted by the following three steps.*

- (1) **Abduction:** Given evidence \mathbf{e} , obtain updated distribution $p(\mathbf{U} | \mathbf{e})$.
- (2) **Action:** Determine feasible intervention $do(\mathbf{C} = \mathbf{c}^*)$ by Feasible Intervention Optimization to achieve change $(\mathbf{A} = \mathbf{a}^*)$ and modify the model into \mathcal{M}_C by cutting off the link between \mathbf{C} and their parents.
- (2) **Prediction:** Compute the probability of \mathbf{B} , the counterfactual consequence, using the updated model $\langle \mathcal{M}_C, p(\mathbf{U} | \mathbf{e}) \rangle$.

F. Differences between Natural Counterfactuals and Non-Backtracking Counterfactuals (Pearl, 2009) or Prior-Based Backtracking Counterfactuals (von Kügelgen et al., 2022)

F.1. Differences between Non-backtracking Counterfactuals and Ours

Non-backtracking counterfactuals only do a direct intervention on target variable \mathbf{A} , while our natural counterfactuals do backtracking when the direct intervention is infeasible. Notice that when the direct intervention on \mathbf{A} is already feasible, our procedure of natural counterfactuals will be automatically distilled to the non-backtracking counterfactuals. In this sense, non-backtracking counterfactual reasoning is our special case.

F.2. Differences between Prior-Based Backtracking Counterfactuals and Ours

(1) Intervention Approach and Resulting Changes:

Prior-based Backtracking Counterfactuals: These counterfactuals directly intervene on noise/exogenous variables, which can lead to unnecessary changes in the counterfactual world. Consequently, the similarity between the actual data point and

its counterfactual counterpart tends to be lower. In short, prior-based backtracking counterfactuals may introduce changes that are not needed.

Natural Counterfactuals: In contrast, our natural counterfactuals only engage in necessary backtracking when direct intervention is infeasible. This approach aims to ensure that the counterfactual world results from minimal alterations, maintaining a higher degree of fidelity to the actual world.

(2) Counterfactual Worlds:

Prior-based Backtracking Counterfactuals: This approach assigns varying weights to the numerous potential counterfactual worlds capable of effecting the desired change. The weight assigned to each world is directly proportional to its similarity to the actual world. It is worth noting that among this array of counterfactual worlds, some may exhibit minimal resemblance to the actual world, even when equipped with complete evidence, including the values of all endogenous variables. This divergence arises because by sampling from the posterior distribution of exogenous variables, even highly dissimilar worlds may still be drawn.

Natural Counterfactuals: In contrast, our natural counterfactuals prioritize the construction of counterfactual worlds that closely emulate the characteristics of the actual world through an optimization process. As a result, in most instances, one actual world corresponds to a single counterfactual world when employing natural counterfactuals with full evidence.

(3) Implementation Practicality:

Prior-based Backtracking Counterfactuals: The practical implementation of prior-based backtracking counterfactuals can be a daunting challenge. To date, we have been prevented from conducting a comparative experiment with this approach due to uncertainty about its feasibility in practical applications. Among other tasks, the computation of the posterior distribution of exogenous variables can be a computationally intensive endeavor. Furthermore, it is worth noting that the paper (von Kügelgen et al., 2022) provides only rudimentary examples without presenting a comprehensive algorithm or accompanying experimental results.

Natural Counterfactuals: In stark contrast, our natural counterfactuals have been meticulously designed with practicality at the forefront. We have developed a user-friendly algorithm that can be applied in real-world scenarios. Rigorous experimentation, involving four simulation datasets and two public datasets, has confirmed the efficacy and reliability of our approach. This extensive validation underscores the accessibility and utility of our algorithm for tackling specific problems, making it a valuable tool for practical applications.

G. Observations about the Prior-Based Backtracking Counterfactuals (von Kügelgen et al., 2022)

G.1. Possibility of Gratuitous Changes

A theory of backtracking counterfactuals was recently proposed by (von Kügelgen et al., 2022), which utilizes a prior distribution $p(\mathbf{U}, \mathbf{U}^*)$ to establish a connection between the actual model and the counterfactual model. This approach allows for the generation of counterfactual results under any condition by considering paths that backtrack to exogenous noises and measuring closeness in terms of noise terms. As a result, for any given values of $\mathbf{E} = \mathbf{e}$ and $\mathbf{A}^* = \mathbf{a}^*$, it is possible to find a sampled value $(\mathbf{U} = \mathbf{u}, \mathbf{U}^* = \mathbf{u}^*)$ from $p(\mathbf{U}, \mathbf{U}^*)$ such that $\mathbf{E}_{\mathcal{M}(\mathbf{u})} = \mathbf{e}$ and $\mathbf{A}^*_{\mathcal{M}^*(\mathbf{u}^*)} = \mathbf{a}^*$, as described in (von Kügelgen et al., 2022). This holds true even in cases where $\mathbf{V} \setminus \mathbf{E} = \emptyset$ and $\mathbf{V}^* \setminus \mathbf{A}^* = \emptyset$, implying that any combination of endogenous values $\mathbf{E} = \mathbf{e}$ and $\mathbf{A}^* = \mathbf{a}^*$ can co-occur in the actual world and the counterfactual world, respectively. In essence, there always exists a path $(\mathbf{v} \rightarrow \mathbf{u} \rightarrow \mathbf{u}^* \rightarrow \mathbf{v}^*)$ that connects $\mathbf{V} = \mathbf{v}$ and $\mathbf{V}^* = \mathbf{v}^*$ through a value $(\mathbf{U} = \mathbf{u}, \mathbf{U}^* = \mathbf{u}^*)$, where \mathbf{v} and \mathbf{v}^* represent any values sampled from $p_{\mathcal{M}}(\mathbf{V})$ and $p_{\mathcal{M}^*}(\mathbf{V}^*)$, respectively.

However, thanks to this feature, this understanding of counterfactuals may allow for what appears to be gratuitous changes in realizing a counterfactual supposition. This occurs when there exists a value assignment $\mathbf{U}^* = \mathbf{u}^*$ that satisfies $\mathbf{E}^*_{\mathcal{M}^*(\mathbf{u}^*)} = \mathbf{e}$ and $\mathbf{A}^*_{\mathcal{M}^*(\mathbf{u}^*)} = \mathbf{a}^*$ in the same world. In such a case, intuitively we ought to expect that $\mathbf{E}^* = \mathbf{e}$ should be maintained in the counterfactual world (as in the factual one). However, there is in general a positive probability for $\mathbf{E}^* \neq \mathbf{e}$. This is due to the existence of at least one ‘‘path’’ from $\mathbf{E} = \mathbf{e}$ to any value \mathbf{v}^* sampled from $p_{\mathcal{M}^*}(\mathbf{V}^* | \mathbf{A}^* = \mathbf{a}^*)$ by means of at least one value $(\mathbf{U} = \mathbf{u}, \mathbf{U}^* = \mathbf{u}^*)$, allowing \mathbf{E}^* to take any value in the support of $p_{\mathcal{M}^*}(\mathbf{E}^* | \mathbf{A}^* = \mathbf{a}^*)$.

In the case where $\mathbf{A}^* = \emptyset$, an interesting observation is that \mathbf{E}^* can take any value within the support of $p_{\mathcal{M}^*}(\mathbf{E}^*)$. Furthermore, when examining the updated exogenous distribution, we find that in Pearl’s non-backtracking framework, it is given by $p_{\mathcal{M}^*}(\mathbf{U}^* | \mathbf{E}^* = \mathbf{e})$. However, in (von Kügelgen et al., 2022)’s backtracking framework, the updated exogenous

distribution becomes $p_B(\mathbf{U}^*|\mathbf{E} = \mathbf{e}) = \int p(\mathbf{U}^*|\mathbf{U})p_{\mathcal{M}}(\mathbf{U}|\mathbf{E} = \mathbf{e})d(\mathbf{U}) \neq p_{\mathcal{M}^*}(\mathbf{U}^*|\mathbf{E}^* = \mathbf{e})$, since using \mathbf{u}^* sampled from $p(\mathbf{U}^*|\mathbf{U} = \mathbf{u})$ (where \mathbf{u} is any value of \mathbf{U}) can result in any value of all endogenous variables \mathbf{V}^* . Therefore, (von Kügelgen et al., 2022)’s backtracking counterfactual does not reduce to Pearl’s counterfactual even when $\mathbf{A}^* = \emptyset$.

G.2. Issues with the Distance Measure

In Equation 3.16 of (von Kügelgen et al., 2022), Mahalanobis distance is used for real-valued $\mathbf{U} \in \mathbb{R}^m$, defined as $d(\mathbf{u}^*, \mathbf{u}) = \frac{1}{2}(\mathbf{u}^* - \mathbf{u})^T \Sigma^{-1}(\mathbf{u}^* - \mathbf{u})$. However, it should be noted that the exogenous variables are not identifiable. There are several issues with using the Mahalanobis distance in this context.

Firstly, selecting different exogenous distributions would result in different distances. This lack of identifiability makes the distance measure sensitive to the choice of exogenous distributions.

Secondly, different noise variables may have different scales. By using the Mahalanobis distance, the variables with larger scales would dominate the distribution changes, which may not accurately reflect the changes in each variable fairly.

Thirdly, even if the Mahalanobis distance $d(\mathbf{u}^*, \mathbf{u})$ is very close to 0, it does not guarantee that the values of the endogenous variables are similar. This means that the Mahalanobis distance alone may not capture the similarity or dissimilarity of the endogenous variables adequately.

H. Another Type of Minimal Change: Minimal Change in Local Causal Mechanisms.

Changes in local mechanisms are the price we pay to do interventions, since interventions are from outside the model and sometimes are imposed on a model by us. Hence, we consider minimal change in local causal mechanisms in \mathbf{A} ’s ancestor set $\mathbf{AN}(\mathbf{A})$. With L^1 norm, the total distance of mechanisms in $\mathbf{AN}(\mathbf{A})$, called **mechanism distance**, is defined as:

$$D(\mathbf{u}_{an(\mathbf{A})}, \mathbf{u}_{an(\mathbf{A})}^*) = \sum_j w_j \|F(\mathbf{u}_j) - F(\mathbf{u}_j^*)\|_1 \quad (9)$$

where $\mathbf{u}_{an(\mathbf{A})}$ is the value of \mathbf{A} ’s exogenous ancestor set $\mathbf{U}_{\mathbf{AN}(\mathbf{A})}$ when $\mathbf{AN}(\mathbf{A}) = an(\mathbf{A})$ in the actual world. $\mathbf{u}_{an(\mathbf{A})}^*$ is the value of $\mathbf{U}_{\mathbf{AN}(\mathbf{A})}$ when $\mathbf{AN}(\mathbf{A}) = an(\mathbf{A})^*$ in the counterfactual world. $D(\mathbf{u}_{an(\mathbf{A})}, \mathbf{u}_{an(\mathbf{A})}^*)$ represents the distance between actual world and counterfactual world. w_j represents a fixed weight, and $F(\cdot)$ is the Cumulative Distribution Function (CDF). We employ the CDF of noise variables to normalize distances across various noise distributions, ensuring these distances fall within the range of $[0, 1]$, as noise distributions are not identifiable.

Weights in the Distance. The noise variables are independent of each other and thus, unlike in perception distance, the change of causal earlier noise variables will not lead the change of causal later noise nodes. Therefore, if the weight on difference of each noise variable is the same, the distance will not prefer less change on variables closer to \mathbf{A} . To achieve backtracking as less as possible, we set a weight w_j for each node \mathbf{U}_j , defined as the number of endogenous decedents of \mathbf{V}_j denoted as $ND(\mathbf{V}_j)$. Generally speaking, for all variables causally earlier than \mathbf{A} , one way is to use the number of variables influenced by particular intervention as the measure of the changes caused by the intervention. Hence, the number of variables influenced by a variable’s intervention can be treated as the coefficient of distance. For example, in a causal graph where where \mathbf{B} causes \mathbf{A} and \mathbf{C} is the confounder of \mathbf{A} and \mathbf{B} . If $change(\mathbf{A} = \mathbf{a}^*)$, $\mathbf{u}_{\mathbf{A}}$ ’s and $\mathbf{u}_{\mathbf{B}}$ ’s weight is 1 and 2 respectively. In this way, variables (e.g., $\mathbf{u}_{\mathbf{B}}$) with bigger influence on other variables possess bigger weights and thus tend to change less, reflecting necessary backtracking.

H.1. Concretization of Natural Counterfactuals: An Example Methodology

A Method Based on Mechanism Distance. We plugin mechanism distance Eqn. 9 into FIO framework Eqn. 2. Below is the equation of optimization:

$$\begin{aligned} \min_{\mathbf{u}_{an(\mathbf{A})}^*} & \sum_j w_j \|F(\mathbf{u}_j) - F(\mathbf{u}_j^*)\|_1 \\ s.t. & \mathbf{a}^* = f_A(pa_{\mathbf{A}}^*, \mathbf{u}_{\mathbf{A}}^*) \\ s.t. & \epsilon < F(\mathbf{u}_j^*) < 1 - \epsilon, \forall \mathbf{u}_j^* \in u_{an(\mathbf{A})}^* \end{aligned} \quad (10)$$

Where the first constraint is to achieve $change(\mathbf{A} = \mathbf{a}^*)$, the second constraint require counterfactual data point to satisfy ϵ -natural generation given the optional naturalness criteria (3) in Sec. 4.2, and the optimization parameter is the value

$\mathbf{u}_{an(\mathbf{A})^*}$ of noise variable set $\mathbf{U}_{AN(\mathbf{A})}$ given $\mathbf{AN}(\mathbf{A}) = an(\mathbf{A})^*$. For simplicity, we use \mathbf{A} as subscript as indicator of terms related to \mathbf{A} , instead of number subscript. In practice, the Lagrangian method is used to optimize our objective function. The loss is as below:

$$\begin{aligned} \mathcal{L} &= \sum_j w_j \|F(\mathbf{u}_j) - F(\mathbf{u}_j^*)\|_1 \\ &+ w_\epsilon \sum_j \max((\epsilon - F(\mathbf{u}_j^*), 0) + \max(\epsilon + F(\mathbf{u}_j^*) - 1, 0)) \\ \text{s.t. } &\mathbf{u}_{\mathbf{A}}^* = f_{\mathbf{A}}^{-1}(\mathbf{a}^*, pa_{\mathbf{A}}^*) \end{aligned} \quad (11)$$

In the next section, we use Eqn. 11 for feasible intervention optimization across multiple machine learning case studies, showing that mechanism distance is as effective as perception distance, as discussed in the main paper.

H.2. Case Study

H.2.1. MORPHOMNIST

Table 12. MorphoMNIST results of $change(i)$ or $do(i)$ using V-SCM

Intersection between Ours and NB		(NCO=1, NB=1)	(NCO=1, NB=0)	(NCO=0, NB=1)	(NCO=0, NB=0)
Number of Intersection		5841	3064	0	1094
Nonbacktracking	t 's MAE	0.286	0.159	0.462	0.000
	i 's MAE	6.62	4.00	8.88	0.000
Ours	t 's MAE	0.175	0.159	0.206	0.000
	i 's MAE	4.41	4.00	5.19	0.000

In this section, we study two types of counterfactuals on the dataset called MorphoMNIST, which contains three variables (t, i, x) . From the causal graph shown in Fig. 12 (a), t (the thickness of digit stroke) is the cause of both i (intensity of digit stroke) and x (images) and i is the direct cause of x . Fig. 12 (b) shows a sample from the dataset. The dataset contains 60000 images as the training set and 10000 as the test set.

We follow the experimental settings of simulation experiments in Sec. 6.1, except for two differences. One is that we use two state-of-the-art deep learning models, namely V-SCM (Pawlowski et al., 2020) and H-SCM (Ribeiro et al., 2023), as the backbones to learn counterfactuals. They use normalizing flows to learn causal relationships among x 's parent nodes, e.g., (t, i) in MorphoMNIST. Further, to learn $p(x|t, i)$, notice that V-SCM uses VAE (Kingma & Welling, 2014) and HVAE (Maaløe et al., 2019). Another difference is that, instead of estimating the outcome with MAE, we follow the same metric called counterfactual effectiveness in Ribeiro et al. (2023) developed by Monteiro et al. (2023). First, trained on the dataset, parent predictors given a value of x can predict parent values, i.e., (t, i) 's, and then measure the absolute error between parent values after hard intervention or feasible intervention and their predicted values, which is measured on image the Learned SCM generates given the input of (t, i) .

Table 13. Ablation Study on ϵ

Model	ϵ	CFs	do(t)		do(i)	
			t	i	t	i
V-SCM	-	NB	0.336	4.51	0.286	6.62
	10^{-4}	Ours	0.314	4.48	0.197	4.90
	10^{-3}		0.297	4.47	0.175	4.41
	10^{-2}		0.139	4.35	0.151	3.95
H-SCM	-	NB	0.280	2.54	0.202	3.31
	10^{-4}	Ours	0.260	2.49	0.117	2.23
	10^{-3}		0.245	2.44	0.103	2.03
	10^{-2}		0.0939	2.34	0.0863	1.87

Quantitative Results of $change(i)$ or $do(i)$. We use V-SCM to do counterfactual task of $change(i)$ (where $\epsilon = 10^{-3}$) or $do(i)$ with multiple random seeds on test set. In Table 12, the first column shows the MAE of (t, i) , indicating our results

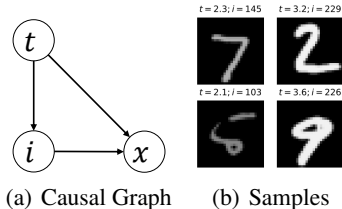


Figure 12. Causal Graph and samples of Morpho-MNIST.

Table 14. Results on Weak-3DIdent and Stong-3DIdent

Dataset	Counterfactuals	d	h	v	γ	α	β	b
Weak-3DIdent	Nonbacktracking	0.0252	0.0191	0.0346	0.364	0.266	0.0805	0.00417
	Ours	0.0241	0.0182	0.0339	0.348	0.224	0.0371	0.00416
Stong-3DIdent	Nonbacktracking	0.104	0.0840	0.0770	0.385	0.495	0.338	0.00476
	Ours	0.0633	0.0512	0.0518	0.326	0.348	0.151	0.00464

outperform that of non-backtracking. Next, we focus on the rest four-column results. In both types of counterfactuals, we use the same value i in $do(i)$ and $change(i)$. Hence, after inference, we know which image satisfying ϵ -natural generation in the two types of counterfactuals. In "NC=1" of the table, NC indicates the set of counterfactuals after feasible intervention optimization. Notice that NC set does not mean the results of natural counterfactuals, since some results do still not satisfy ϵ -natural generation after feasible intervention optimization. "NC=1" mean the set containing data points satisfying ϵ -natural generation and "NC=0" contains data not satisfying ϵ -natural generation after feasible intervention optimization. Similarly, "NB=1" means the set containing data points satisfying naturalness criteria. (NC=1, NB=1) presents the intersection of "NC=1" and "NB=1". Similar logic is adopted to the other three combinations. The number of counterfactual data points are 10000 in two types of counterfactuals.

In (NC=1, NB=1) containing 5841 data points, our performance is similar to the non-backtracking, showing feasible intervention optimization tends to backtrack as less as possible when hard interventions have satisfied ϵ -natural generation. In (NC=1, NB=0), there are 3064 data points, which are "unnatural" points in non-backtracking counterfactuals. After natural counterfactual optimization, this huge amount of data points become "natural". In this set, our approach contributes to the maximal improvement compared to the other three sets in Table 12, improving 55.4% and 41.6% on thickness t and intensity i . The number of points in (NC=0, NB=1) is zero, showing the stability of our algorithm since our approach will not move the hard, feasible intervention into an unfeasible intervention. Two types of counterfactuals perform similarly in the set (NC=0, NB=0), also showing the stability of our approach.

Ablation Study on Naturalness Threshold ϵ . We use two models, V-SCM and H-SCM, to do counterfactuals with different values of ϵ . As shown in Table 13, our error is reduced as the ϵ increases using the same inference model, since the higher ϵ will select more feasible interventions.

H.2.2. 3DIDENTBOX

In this task, we utilize practical public datasets called 3DIdentBOX, which encompass multiple datasets (Bizeul et al., 2023). Specifically, we employ Weak-3DIdent and Strong-3DIdent, both of which share the same causal graph depicted in Fig. 13 (a), consisting of an image variable denoted as x and seven parent variables. These parent variables, denoted as (d, h, v) , control the depth, horizon position, and vertical position of the teapot in image x respectively. Additionally, the variables (γ, α, β) govern three types of angles associated with the teapot within images, while variable b represents the background color of the image. As illustrated in Fig. 13 (a), causal relationships exist among three pairs of parent variables, i.e., (h, d) , (v, β) and (α, γ) . It is important to note a distinction between Weak-3DIdent and Strong-3DIdent. In Weak-3DIdent, there exists a weak causal relationship between the variables of each pair, as shown in Fig. 13 (b), whereas in Strong-3DIdent, the causal relationship is stronger, as depicted in Fig. 13 (c).

We follow the same experimental setup as in the MophoMNIST experiments. Using an epsilon value of $\epsilon = 10^{-3}$ we employ the H-SCM as the inference model. We conduct interventions or changes on the variables (d, β, γ) and the results are presented in Table 14. In both datasets, our approach outperforms the non-backtracking method, with Strong-3DIdent

exhibiting a more significant margin over the non-backtracking method. This is because the non-backtracking method encounters more unfeasible interventions when performing hard interventions using Strong-3DIdent.

Additionally, we perform visualizations on Strong-3DIdent. In Fig. 14, we display counterfactual outcomes in (a) and (b), where the text above each image in the first row (evidence) indicates the error in the corresponding counterfactual outcome shown in the second row. In Fig. 14 (a), we present counterfactual images that do not meet the ϵ -natural generation criteria in the non-backtracking approach. In contrast, Fig. 14 (b) showcases our results, which are notably more visually effective. This demonstrates that our solution can alleviate the challenges posed by hard interventions in the non-backtracking method.

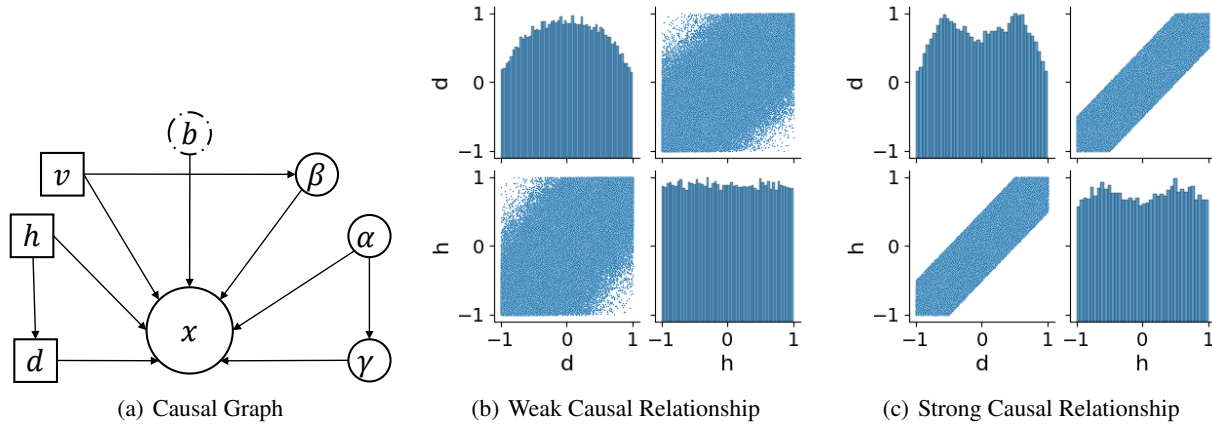
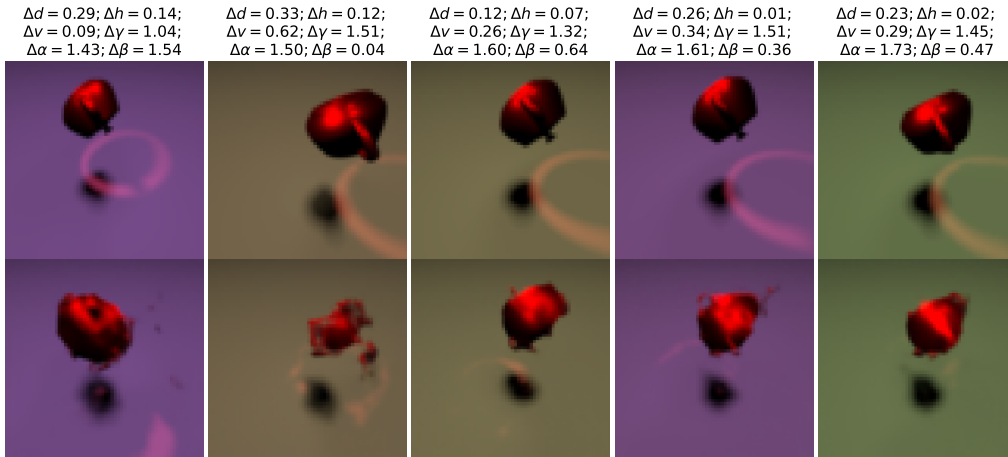
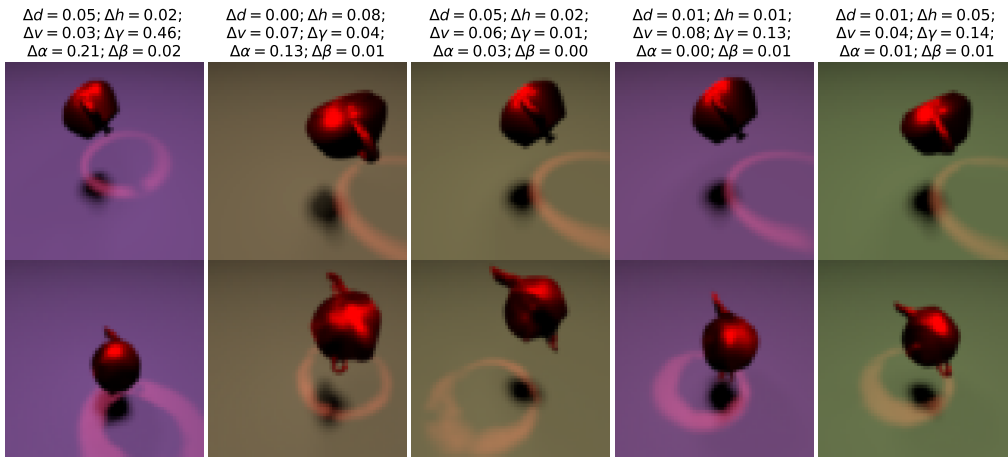


Figure 13. Causal graph of 3DIdent and the causal relationships of variables (d, h) in Weak-3DIdent and Strong-3DIdent respectively.



(a) Results of Non-backtracking Counterfactuals



(b) Results of Natural Counterfactuals

Figure 14. Visualization Results on Stong-3DIdent.